Progress in Energy and Combustion Science 62 (2017) 133–154

Contents lists available at ScienceDirect

Progress in Energy and Combustion Science

journal homepage: www.elsevier.com/locate/pecs

Continuous-flow electroreduction of carbon dioxide

B. Endrődi[a,b], G. Bencsik[a,b], F. Darvas[c], R. Jones[c], K. Rajeshwar[d], C. Janáky[a,b,*]

[a] MTA-SZTE "Lendület" Photoelectrochemistry Research Group, Rerrich Square 1, Szeged, H-6720, Hungary
[b] Department of Physical Chemistry and Materials Science, University of Szeged, Rerrich Square 1, Szeged, H-6720, Hungary
[c] ThalesNano Inc., Záhony u. 7, Budapest 1031, Hungary
[d] Department of Chemistry and Biochemistry, University of Texas at Arlington, Arlington, TX 76019, USA

ARTICLE INFO

Article History:
Received 23 February 2017
Accepted 31 May 2017
Available online 13 June 2017

Keywords:
Electrolysis
CO_2 conversion
Renewable energy
Syngas
Solar fuels

ABSTRACT

Solar fuel generation through electrochemical CO_2 conversion offers an attractive avenue to store the energy of sunlight in the form of chemical bonds, with the simultaneous remediation of a greenhouse gas. While impressive progress has been achieved in developing novel nanostructured catalysts and understanding the mechanistic details of this process, limited knowledge has been gathered on continuous-flow electrochemical reactors for CO_2 electroreduction. This is indeed surprising considering that this might be the only way to scale-up this fledgling technology for future industrial application. In this review article, we discuss the parameters that influence the performance of flow CO_2 electrolyzers. This analysis spans the overall design of the electrochemical cell (microfluidic or membrane-based), the employed materials (catalyst, support, etc.), and the operational conditions (electrolyte, pressure, temperature, etc.). We highlight R&D avenues offering particularly promising development opportunities together with the intrinsic limitations of the different approaches. By collecting the most relevant characterization methods (together with the relevant descriptive parameters), we also present an assessment framework for benchmarking CO_2 electrolyzers. Finally, we give a brief outlook on *photo*electrochemical reactors where solar energy input is directly utilized.

Contents

Abbreviations: BID, Barrier ionization discharge detector; CO_2, Carbon dioxide; R_{cell}, Cell resistance; R_{ct}, Charge transfer resistance; CB, Conduction band; CV, Cyclic voltammetry; DEMS, Differential electrochemical mass spectrometry; EIS, Electrochemical impedance spectroscopy; EC, Electrochemical; EDX, Energy-dispersive X-ray spectroscopy; FE, Faradaic efficiency; FT-IR, Fourier transform infrared spectroscopy; GC, Gas chromatography; GDEs, Gas diffusion electrodes; GDL, Gas diffusion layer; LSV, Linear sweep voltammetry; MEAs, Membrane electrode assemblies; NMR, Nuclear magnetic resonance; OER, Oxygen evolution reaction; PC, Photochemical; PEC, Photoelectrochemical; PV, Photovoltaic; PVA, Poly(vinyl alcohol); PEM, Polymer electrolyte membrane; SEM, Scanning electron microscopy; SC, Semiconductor; STH, Solar-to-hydrogen; SOE, Solid-oxide electrolyzers; Rs, Solution resistance; SCCM, Standard cubic centimeters per minute; SPEEK, Sulfonated poly(ether ether ketone); 3D, Three-dimensional; TEM, Transmission electron microscopy; UV, Ultraviolet; R_u, Uncompensated resistance; VB, Valence band; XRF, X-ray fluorescence spectroscopy; XPS, X-ray photoelectron spectroscopy; XRD, X-ray powder diffraction

* Corresponding author.
E-mail address: janaky@chem.u-szeged.hu (C. Janáky).

http://dx.doi.org/10.1016/j.pecs.2017.05.005

1. Introduction

Finding adequate solutions for a diversified and sustainable energy supply is undoubtedly one of the grand challenges of our society today [1]. It is imperative that renewable energy sources and solar/wind energy in particular, are increasingly used to improve the security of energy supplies and also ameliorate the environmental impact from carbon-based energy production and consumption. While solar and wind electricity generation already enjoy an important, and impressively increasing role in the global (and especially European) energy mix, *storage* is still an issue because of the intermittency of most renewable energy sources [2]. At the same time, the steeply rising level of carbon dioxide (CO_2) in the atmosphere calls for conceptually new approaches to capture and utilize this greenhouse gas. A solar fuels-based economy tackles the above parallel challenges admirably well, although many challenges remain before widespread use of such energy carriers (e.g., H_2, methanol, ethanol, and methane) sees the light of day.

CO_2 is a greenhouse gas; therefore using renewable energy to convert CO_2 to transportation fuels and commodity chemicals is a value-added approach to simultaneous generation of products and environmental remediation of carbon emissions. The large amounts of chemicals produced worldwide (Fig. 1) that can be potentially derived from the hydrogenation of CO_2, highlights further the importance of this strategy. Several industrial entities are interested in such technologies, ranging from energy/utilities companies through cement producing and processing firms to oil and gas companies.

There are numerous routes for converting CO_2 to transportation fuels and other chemicals. The following three major pathways delineate how *sunlight* can be used to generate such products (e.g., CH_4 or CH_3OH) from CO_2 (Fig. 1) [2–7].

Photochemical (PC) or photosynthetic methods: Directly use sunlight to photochemically convert CO_2 to fuels using molecular- or suspended semiconductor (SC) photocatalysts [8–10].

Electrochemical (EC) approaches: Here sunlight is first converted to electricity by a photovoltaic solar cell (PV) and CO_2 is then reduced electrochemically [11,12].

Photoelectrochemical (PEC) route: Photogenerated electrons are utilized to reduce CO_2 either directly at a SC/electrolyte interface or indirectly employing a redox mediator [13].

With the recent rapid drop in the cost of Si solar cells, the price of solar electricity has decreased to a level that in over 20 countries translates to grid parity. A recent study concluded that on a 20–25 year term it is not likely that any solar energy utilization pathways other than Si solar photovoltaic panels will have an industrially-relevant role [14]. Another techno-economic analysis suggested that PV+EC conversion setups may attain ~14% solar to H_2 efficiency (20% PV, 70% EC) in an economically feasible manner as the electricity price drops (which is clearly the case for both solar and wind power) [4]. These factors suggest that CO_2 conversion, at least on a short to intermediate term, will be driven in an EC configuration (note also the availability of other renewable electricity sources, such as wind). On a longer term basis, the PEC strategy also cannot be ruled out and in fact, further extensive research work is highly encouraged [4].

Electrochemical (EC) and photoelectrochemical (PEC) conversion of CO_2 are multi-electron in nature (up to 8 e^- for conversion to methane) with considerable kinetic barriers to electron transfer. It therefore requires the use of carefully designed electrode surfaces to accelerate electron transfer rates to levels that make practical sense. In this vein, much has been written about the electrochemical, solid-state physics, theoretical, catalytic, and general materials science aspects of EC/PEC CO_2 reduction [15–17]. During the past 5 years, however, an accelerated progress has occurred, reflected in the number of published research articles and the citations they attracted (Fig. 2). Most of this work has focused on the development of new catalysts [18] and the enhancement of product selectivity [11,19]. Excitingly, we appear to be at the very cusp of a new era of electrochemical CO_2 conversion studies, which hopefully will lead to efficient CO_2 electrolyzers on a practical scale.

At this juncture, however, it has to be noted that CO_2 reduction is a lot more complex than water splitting, simply because many different products can be formed via proton-coupled multi-electron transfer [20]. To drive this process in an economically attractive way, it is important to produce (i) any product as selectively as possible; (ii) products of economic value; and (iii) products that are easy to separate. A recently-performed techno-economic analysis on the process suggested that the picture is even murkier, because co-producing a low value product (such as methanol or ethylene) together with a high value product (such as formic acid or carbon-monoxide) can be a better strategy than producing them alone. In fact, the optimal scenario would be to co-produce two products that are in different phases (i.e., one in the liquid phase and the other in the gas phase) as the separation process becomes straightforward in this case [21].

In addition, since the redox potential for proton to H_2 transformation is very close to the redox potential of the desired CO_2 reduction processes, there is always a competition between these two processes. Furthermore, although thermodynamic considerations would allow reduction of CO_2 at moderately negative potentials, electrochemical reduction of CO_2 is kinetically daunting with high overpotentials needed for its conversion to hydrocarbons and alcohols. Finally, in a simple batch reactor, the maximum achievable rate

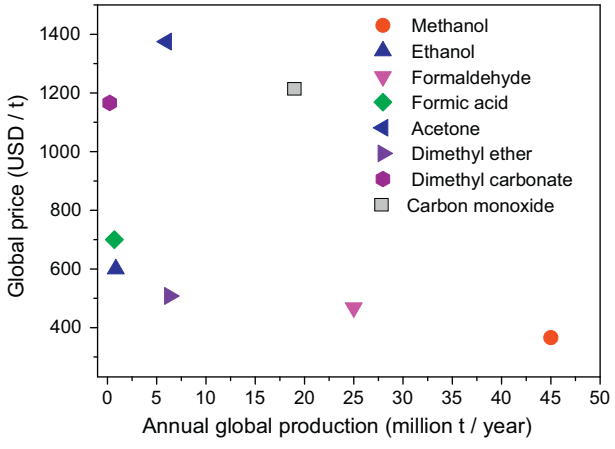

Fig. 1. Global market of the most important CO_2-utilization products.

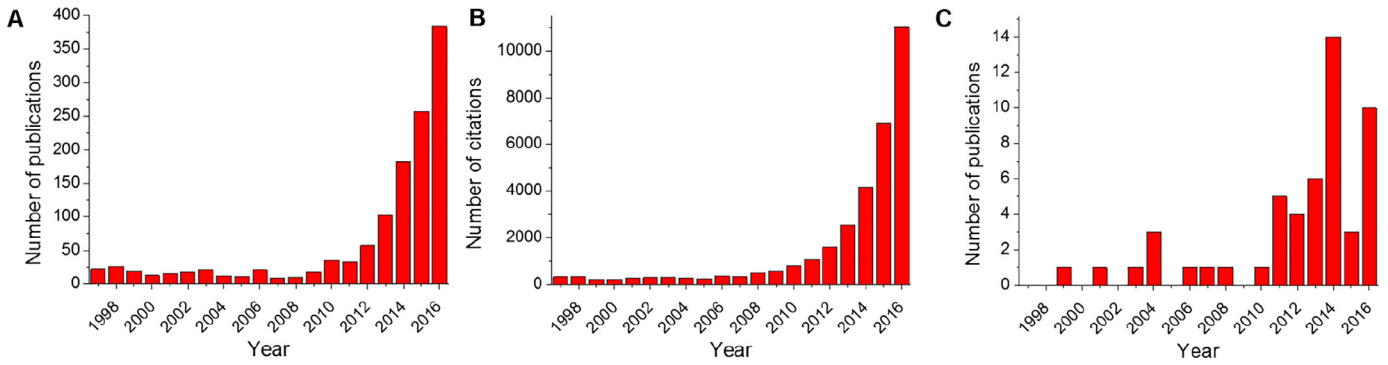

Fig. 2. Results of a literature survey on electrochemical and photoelectrochemical CO_2 reduction. A: number of papers published, B: the citations gathered by these papers, C: papers claimed to use a flow-setup (this is a subset of Fig. 2A).

for the reaction is often limited by the low solubility (~30 mM) of CO_2 in water. Using a simple semi-infinite diffusion model, the limiting current density attainable at this concentration is approximately $I_L = 60\ mA\ cm^{-2}$ under vigorous stirring [22]. Importantly, the solubility of CO_2 strongly depends on the temperature, the solution pH, and the ionic strength as well, which should be taken into account when comparing data measured in different solutions [23].

To increase the CO_2 conversion rate to a level of practical significance, EC CO_2 reduction must be performed in a continuous-flow setup to overcome mass-transport limitations. We note that there is a striking difference here compared to water splitting, where ample amounts of water molecules (55.5 M!) are available for the reaction. Interestingly, despite some successful pioneering studies [24], very little attention has been devoted to EC CO_2 reduction *in continuous flow mode*. Only a minor fraction (~5%) of the articles (see Fig. 2C) report on studies performed under such flow conditions. In fact, this trend can also be very problematic in the sense that conclusions drawn from batch experiments cannot be directly translated to flow situations (unlike for water splitting).

There are a few reviews on electrochemical cell designs for CO_2 reduction: namely microfluidic reactors [25,26] and polymer electrolyte membrane (PEM) electrolyzers [27]. Solid-oxide electrolyzers, while an important category, fall outside the purview of the present study, because of their vastly different operational principles and conditions (high temperature, single CO product, etc.) [28]. In a continuous flow CO_2 electrolyzer, multiple parameters have to be simultaneously tailored to possibly achieve an economically viable process [21]. In two recent articles careful modeling on the effect of the various operational parameters (pH, concentration, temperature) was carried out, mostly through studying the CO_2/carbonate family equilibrium [29,30]. In this review, we focus on real operational cells: materials aspects, device-related features, together with operational parameters are the three main categories forming the crux of this article. We compare various reports in the literature, to identify the role of the individual parameters, and to set guidelines for future studies. We also incorporate the lessons learned from the fuel cell and water electrolyzer communities, while highlighting also the most important differences.

The prematurity of the field is also reflected in the lack of precise definition of electrochemical flow cells. A simple literature search for "flow-electrochemical cell" or "continuous-flow electrolyzer" can easily mislead the reader. For example, some studies in which the liquid phase is continuously purged with systematically varied flux of CO_2 during the measurement are claimed to be on "flow" systems. Although very important conclusions can be drawn from these studies on the effect of the different reaction parameters (e.g., gas flow-rate, electrode composition, pH), these setups significantly differ from those – constituting the core of this study – in which a fresh solution/gas phase is fed to the electrodes continuously as detailed later [31]. Similarly, while in some cases both the catholyte and the anolyte is continuously pumped (and thus refreshed), in other instances only one of them. It is also common that the circumstances of the measurements are not precisely defined, and therefore it is very difficult to determine whether the experiments were performed in a real flow electrolyzer or not.

Finally, in our opinion, there is a strong need for setting the proper measurement protocol for assessing the properties of continuous flow EC cells for CO_2 reduction and for specifying a set of parameters for benchmarking purposes. Such an exercise is particularly relevant because researchers from diverse specialties (e.g., heterogeneous/homogeneous catalysis, fuel cells, water splitting, etc.) and even disciplines (chemistry, physics, and engineering) have congregated in the EC CO_2 reduction arena. These disparate communities often use very different terminologies. Hark back to the history of the fuel cells and water electrolyzer communities where it took decades to establish generally-accepted testing protocols and benchmarking parameters. In the interim period, literally hundreds/thousands of reports accumulated in the literature describing results that could not be reliably intercompared with one another.

2. Reactor designs

Whether we consider technology scale-up or reliable rapid screening of materials in the laboratory, continuous-flow reactors have multiple benefits compared to their batch counterparts. Among others, these include increased mass transfer and improved mixing of different phases, better temperature and heat transfer control, and more precise influence on reaction mixture residence time in the reactor [32]. When moving from batch-type experiments to continuous-flow cells, the architecture and design of the reactor (electrochemical cell) must be first clearly defined. Note that this includes: the type of electrolyte used (liquid/gas), reactor material-reaction mixture compatibility, whether it can be pressurized or not, the applicable temperature and flow rate, and the possibility of using a reference electrode.

Schematic drawings of the most frequently studied cell configurations are presented in Fig. 3. Before discussing each of them individually, we would like to emphasize the importance of the number of electrodes employed in the setup. Many designs only involve two electrodes (a working and a counter electrode); thus only current or *voltage* (not potential) control is possible in these cases. There is a considerable number of electrolyzer setups where a reference electrode is also integrated into the cell, close to the working electrode surface, to ensure the possibility of *potential* control. A four-electrode setup is also possible (with two reference electrodes), if the water oxidation step is complicated, and thus the monitoring of both half-cells becomes important. Potential control is especially important in electrolyzers in which the catalysts (e.g., copper oxides [20]) change their chemical composition (or surface properties)

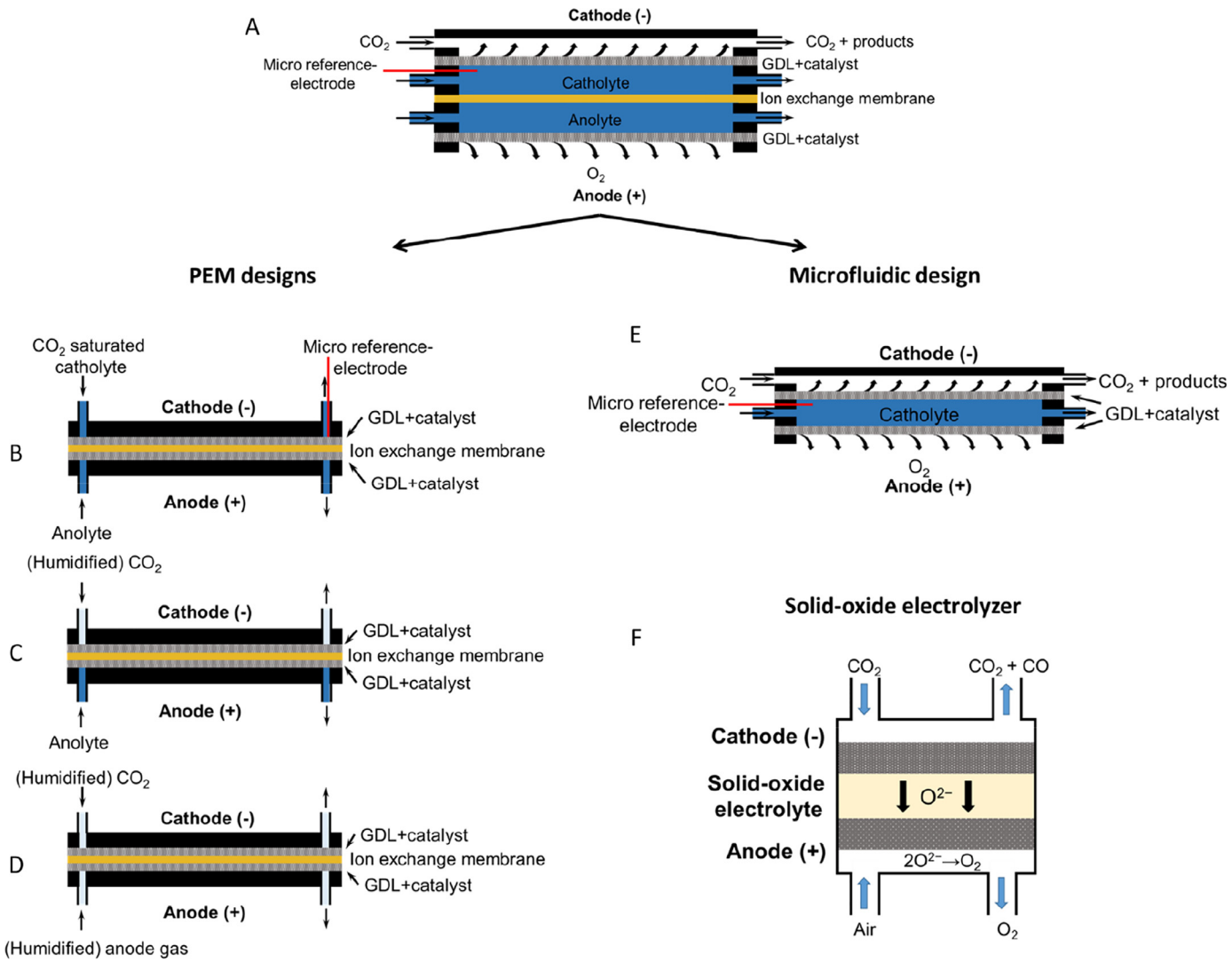

Fig. 3. Sketch and operating principle of the most frequently studied cell configurations in continuous-flow EC CO_2 reduction. (A): general design used to derive: a classical microfluidic setup (E), and three different configurations containing a polyelectrolyte membrane (B–D). (GDL: gas diffusion layer) F: Solid-oxide electrolyzer.

during operation (i.e., aging). This often results in a change in the product distribution with time, as discussed in what follows.

Fig. 3A shows the most universal architecture, from which all other setups can be derived. This parent configuration consists of two flow channels, one for the anolyte and another for the catholyte, separated by an ion-exchange membrane. The cathode electrocatalyst is immobilized on a gas diffusion layer (GDL), which is in contact with the flowing catholyte from one side, while CO_2 gas is directly fed on the other side [33]. This arrangement overcomes most of the problems associated with the other setups, namely: (i) current limitation due to the low concentration of CO_2 at the electrode; (ii) H^+ crossover from the anode and the consequent acidification of the catholyte; (iii) difficulty of inserting a reference electrode; (iv) diffusion of liquid-phase products to the anode, where they are oxidized (product crossover). Although no such instrument is commercially available on the industrial scale at the moment, most components of this setup (i.e., GDLs and catalysts) are available and ready for scale-up already. We note here that it seems to be very challenging to build large stacks based on this concept mostly because of the pressure sensitivity of this structure [34]. We expect therefore that the parallel operation of these instruments (the scale-out concept) will constitute the main track of industrialization in this case – at least in the near future. The other experimental devices (Fig. 3B–E) can be derived by "removing" different elements of this general setup, thus simplifying the overall architecture. By applying a single, undivided channel for flow of the common electrolyte, we get a typical microfluidic reactor (Fig. 3E). In this setup, the electrodes are separated by a thin spacer (usually well below 1 mm in thickness) and no membrane is included [35–39]. The reference electrode can be inserted in the electrolyte flow stream and the excess protons formed on the anode are drained from the cathode vicinity by electrolyte flow (although not as effectively as in the case of separated electrolyte channels).

A popular class of devices feature separation of the two electrodes by an ion-exchange membrane (typically Nafion™, but see also Section 3.5. for others) (Fig. 3B–D). Usually the electrodes are pressed together and no flow channels are formed between them (zero gap cells). The electrolyte/gas is fed to the electrodes (mostly gas diffusion electrodes (GDEs), formed by immobilizing the catalyst on a GDL), and remains in the cell until reaching the exit point. The greatest advantage of these setups, compared to the microfluidic arrangements, is that it is relatively easy to pressurize the reactant and product flows. Furthermore, based on the similarity of these devices to PEM water electrolyzers, the scale-up of these setups to the industrial scale and construction of large sized stacks seems to be more straightforward.

Variants of these setups differ in the type of electrolytes used. The reactants fed to the cathode and anode compartment can be (i) both

in liquid phase (Fig. 3B) [40]; (ii) CO_2 gas on the cathode and liquid phase anolyte (Fig. 3C) [41,42]; (iii) humidified gases on both electrodes (Fig. 3D) [43,44]. Although this may look like a minor difference at first sight, the reactant type has an important and complex effect on cell performance. When feeding pure CO_2 to the cathode, the reactant concentration remains very high on the catalyst, and therefore high reaction rate (current) can be achieved. In this case however, trustworthy measurement of the individual electrode potentials is far from trivial, although several promising attempts were made with all-gas fuel cells [45–48]. Previous studies have shown that the product distribution changes parallel to continuous ageing of certain catalysts during long-term operation [49,50]. The lack of a reference electrode complicates this situation even more, since in this case the change in the cell voltage/current stems from either anode or cathode degradation (or both), whose effects cannot be separated.

The main drawback of these membrane-separated zero-gap devices paradoxically is the same as their main advantage, namely the proximity of the two electrodes to one another. This decreases the cell resistance and consequently, the IR-drop to a minimum level, but on the other hand, ion exchange leads to acidification of the catholyte and therefore to increased production of H_2 (instead of reduction of CO_2). Including a buffer layer between the electrodes can circumvent this effect, but at the same time, leads to increased cell resistance [51]. Although most studies on PEM CO_2 electrolyzers focus on the use of cation exchange membranes, anion exchange membranes may also bear considerable scope in CO_2 conversion. In such arrangements, OH^- ions are transported through the membrane, which results in a different product distribution compared to cation exchange membrane containing systems [52]. A new anion-exchange membrane based electrolyzer was recently developed for both CO_2 conversion and water splitting [53]. The reactors, using the new anion exchange membrane based on polymers containing imidazolium and pyridinium groups, exhibited high durability at industrially relevant current densities (100 mA cm^{-2} for CO formation) [53]. Detailed discussion on the role of the ion-exchange membrane is given in Section 3.5.

It is very important to underline that for industrial applications, large-sized, multiple-stack electrolyzers are required. The current status of this field is very far from this level, since aside from a few examples, all studies were carried out on 1–10 cm^2 sized electrodes [54,55]. Consequently, a grand challenge for future research and development is to construct experimental setups that can be readily translated to *real* industrial technologies.

The operational principle of solid oxide electrolyzers is shown in Fig. 3F. Detailed discussion however, is omitted because of their completely different properties compared to both their microfluidic and PEM counterparts [28].

3. Materials

As outlined in the previous section, various device architectures can be used for the continuous-flow electroreduction of CO_2. There are certain components, however, which are common to all electrolyzer designs, and they are discussed in what follows (also see Table 1 for an overview).

3.1. Electrocatalysts

As it dictates both the kinetics and thermodynamics of the electrolysis process, the electrocatalyst is the heart of such devices. The most extensively scrutinized cathode catalysts and their most important features are summarized in Table 1. When comparing and contrasting these to the catalysts employed in batch experiments we can conclude that (i) the catalyst candidates that proved to be promising in batch setups show similar, or even, higher electrochemical activity in the corresponding flow setup; (ii) the formed products are very similar for both batch and flow experiments; (iii) the reported potential values differ significantly in many cases. The most intensively studied electrocatalysts are Sn, on which formate is produced almost exclusively; Ag with preferred CO formation; and Cu, on which a wide variety of products is formed, depending on the experimental circumstances. Several catalysts (e.g., metal alloys) that were promising in batch experiments however, are still waiting to be tested in flow cells. An example of new generation catalysts is metal organic frameworks (MOFs), which were very recently studied in flow-reactors [56]. Much less effort has been devoted to the anode catalyst, where mostly IrO_x and Pt was employed to facilitate water oxidation (O_2 evolution) [57]. In the outlook section, we present some possible future R&D avenues, where the anode electrocatalyst gets higher importance.

The amount of the electrocatalyst in these devices varies in a relatively broad range, from 0.2 to 10 mg cm^{-2}. The most commonly applied catalyst loading however, is around 1 mg cm^{-2}, independently of the catalyst used. This latter fact is indeed very surprising, since the molar mass, density, and specific surface area of the different catalysts can differ severely. This may cause *several orders of magnitude* difference in the number of electrocatalyst atoms, and more specifically in that of the surface atoms, which can interact with the CO_2 molecules. To get a meaningful comparison on the electrocatalytic properties of different catalysts, one must therefore always normalize the measured current values in terms of either the electrochemically active surface area, or with the number of surface atoms, but not with respect to the geometric surface area or electrode mass. This is even more important in the case of thick porous electrodes, where the current density can be influenced by electrode thickness, without affecting the electrode kinetics.

At this juncture, however we note that researchers need to make sure that all measurements were taken in the kinetically-controlled regime and not the mass transfer-limited regime, before they compare reaction rates across different catalytic systems. Different strategies can be employed to determine mass transfer limitations, for example obtaining breakthrough curves (current density vs. catalyst loading) [78]. An example is shown in Fig. 4, where LSV curves are shown for Sn-based GDEs with different Sn-loading. As seen in Fig. 4A, after a certain Sn-content, the mass-transport limited regime is reached. This trend is directly visualized in Fig. 4B, where the partial current density related to CO_2 reduction is plotted vs. the catalyst loading (note the constant FE values, confirming that the chemical process is identical).

It should also be noted that although attempts were made to directly compare the results of batch experiments with those measured in flow setups, such a comparison is not straightforward because of several reasons [33]. The continuously refreshed solution, reaching the electrode surface leads to striking differences as it has a massive influence on the (i) mass-transport (diffusion layer thickness); (ii) local pH effects; (iii) product accumulation in the close vicinity of the cathode; (iv) residence time of CO_2 molecules at the electrode surface. When applying (humidified) CO_2 gas as "catholyte," its effective concentration on the surface is obviously higher than in the case of aqueous solutions, which leads to higher current densities at the same "potential". Here we refer to our earlier point, namely that defining and measuring electrode potential in such arrangements is also problematic.

3.2. Effects of catalyst size and morphology

Particle size effects [79] have not been extensively studied in flow cells; however, there are some nice examples on copper nanoparticles and thin films (3–21 nm thick) [80]. First it was shown that nanoparticulate Cu (n-Cu) behaves differently than Cu foils (Fig. 5A). In addition, from the film thickness dependent methanation Faradaic

Table 1
Materials properties of champion continuous-flow CO_2 electrolyzers.

Catalyst	Catalyst size	Electrocatalyst loading	Electrode support	Electrode thickness	Current density (mA cm^{-2})	Main Products (FE)	Ref.
Ag	<100 nm	0.75 mg cm^{-2}	Sigracet 35 BC	325 μm	100	CO (80–95)	[58]
Ag	–	–	GDE (Silflon, Gaskatel)	n/a	100	CO (30–90)	[59]
Ag	<100 nm	2 mg cm^{-2}	Sigracet 35 BC	325 μm	340	CO (95+)	[39]
Ag	<100 nm	0.2 mg cm^{-2} (+0.8 mg cm^{-2} MWCNT)	Sigracet 35 BC	325 μm	350	CO (95)	[38]
Ag- complex	–	1 mg cm^{-2}	Sigracet 35 BC	325 μm	95	CO (90)	[36]
Ag	–	n/a	GDE (Silflon, Gaskatel)	n/a	275	CO (80)	[60]
Ag	10 nm on TiO_2 nanoparticles	1 mg cm^{-2}	Sigracet 35BC	325 μm	100	CO (90)	[61]
Au	Foil	–	–	–	2.8	CO (92)	[62]
Au	av. 60 nm	–	Porous membrane	–	3–30	CO (38)	[63]
Cu	2–4 μm, 8–15 μm	2 mg cm^{-2}, 10 mg cm^{-2}	Nafion-117	180 μm	15	C_2H_4 (12–13)	[64]
Cu	Plate	–	–	1 mm	20	CH_4 (40)	[19]
Cu	n/a	n/a	Toray TGP-H-120	370 μm	11	CH_4 (5)	[52]
Cu	10–50 nm	1 mg cm^{-2}	Sigracet 35 BC	325 μm	150	CO (57)	[33]
CuO/Cu	20–40 nm	1 mg cm^{-2}	Sigracet 35 BC	325 μm	11	CO (~20), formate (~20)	[65]
Cu_2O/Cu	n/a	2 mg cm^{-2}	Toray TGP-H-120	370 μm	5.4	CH_4 (32)	[66]
Cu_2O or Cu_2O/ZnO	Cu_2O < 5 μm, ZnO < 45 μm	1 mg cm^{-2}	Toray TGP-H-60	190 μm	10	MeOH (42)	[67]
CuO/Cu_2O	Nanorod arrays	–	Cu foil	n/a	20	EtOH (~50)	[68]
Sn	2.39 mm shot and 0.252 mm granules	n/a	Sn sheet	n/a	310	Formate (63–91)	[54]
Sn	0.3 mm (granules)	n/a	Sn sheet	3 mm	300	Formate (60–90)	[55]
Sn	Nanopowder	2–5 mg cm^{-2}	E-TEK "S"-type GDE	n/a	100	Formate (89)	[35]
Sn	Sn-loaded brass mesh	1.5 mg cm^{-2}	GDL: conductive carbon black+PTFE (3:7)	ca. 0.2 mm	17.6	Formate (79)	[69]
Sn/Cu	–	–	30 # or 60 # copper mesh	610 (30 #) and 380 (60 #) μm	130	Formate (86)	[70]
Sn/Cu	Nanoparticles	–	30 # copper mesh	600 μm	100	Formate (13–86)	[71]
SnO_2	Nanoparticles	0.87 mg cm^{-2}	GDE (acetylene black:PTFE 65:35)	n/a	30 (3 V) 120 (6 V)	Formate (74–84)	[72]
Pb	2–5 μm	0.5 mg cm^{-2}	Toray 170	n/a	46	Formate (65)	[73]
Pb	–	5 mg cm^{-2}	Polytetrafluoroethylene - carbon paper	n/a	143–345	Formate (95)	[37,74]
Fe, Cu, Co, Pt, Fe-Co, Fe-Cu, Fe-Co-Cu	Nanoparticles	0.5 mg cm^{-2}	CNT/Sigracet 24 BC	235 μm	20	–	[75]
In	–	–	Cu mesh	n/a	–	Formate (67)	[76]
Pt	3–5 nm	0.4–0.6 mg cm^{-2}	E-TEK carbon cloth	n/a	20	>C5	[77]

efficiency and gravimetric methanation current experiments, it was demonstrated that thin evaporated films behaved like the n-Cu/C electrodes while thick evaporated films behaved like copper foils (Fig. 5B). In this study, it was also suggested that n-Cu was ideal for preparing GDLs with lowered polarization losses, thus maximizing the energy efficiency of the electrolyzer [80].

In another study, Cu electrodes with different morphologies were prepared [81]. The first important observation was that higher active surface area resulted in an improved total FE compared to the smooth Cu plate. As for the product selectivity: (i) electroplated Cu (on Cu foil) favored the production of formate; (ii) electrofaceting of the Cu foil moved the selectivity towards CH_4 formation; (iii) deposition of Cu onto carbon cloth resulted in the formation of C_2H_4 [81]. The effect of tin loading and particle size were studied in a filter-press cell for CO_2 reduction [82]. Tin particles of different sizes (150 nm, 10 μm, and 150 μm) were studied, and certain size effects were reported with an optimal behavior for the smallest particles. Again, meaningful normalization is a mandatory exercise in such studies, to deconvolute the simple surface area effect from other, chemical underpinnings.

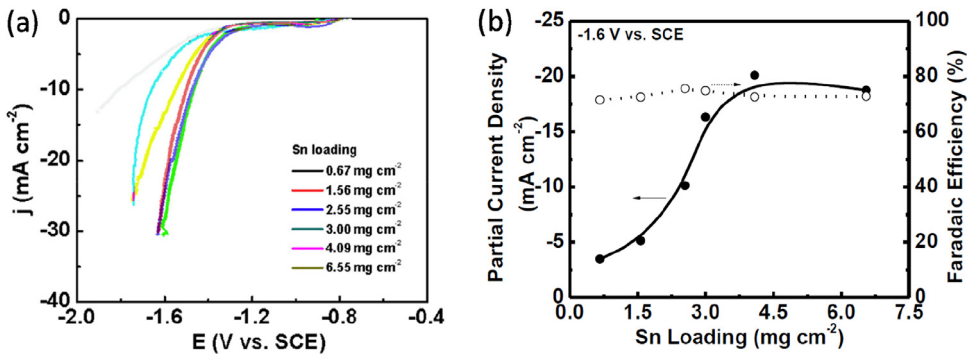

Fig. 4. Current density vs. catalyst loading curves for a Sn/C gas diffusion electrode. Adapted with permission from ref. [78].

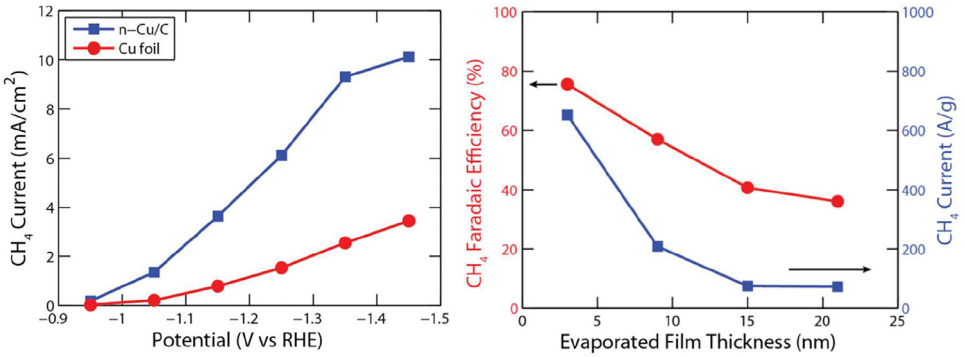

Fig. 5. The effect of Cu film thickness on the Faradaic efficiency and specific current density of CH_4 formation in a continuous-flow electrolyzer. Reproduced with permission from ref. [80].

3.3. Role of the catalyst support

To achieve current densities of practical relevance, it is vital to increase the electroactive surface area of the electrocatalyst. Moreover, in the case of flow electrolyzers, one must also consider that the electrolyte flow continuously removes the products (or intermediates) from the electrode surface, leading to relatively short remanence time. This severely influences both the Faradaic efficiency and product distribution. Therefore, the CO_2 containing electrolyte must be forced to travel through a long path, while it remains in contact with the electrocatalyst for a sufficiently long time period. This can be achieved by immobilizing the catalyst on a GDL, which is a porous substrate with large surface area. The GDL has a dual function in the cell by allowing transport of materials between the catalyst and the flow channel while also maintaining proper electronic communication between the current collector and the electrocatalyst. The most frequently (almost exclusively) applied GDLs are porous carbon supports, formed from carbon fibers or pressed carbon particles. These carbon cloths and carbon papers are frequently used supports in fuel cells and water electrolyzers on the cathode side. Interestingly, although several attempts were made to employ different metal foils or meshes as catalyst supports in CO_2 flow electrolysis cells, the use of different carbonaceous substrates is reported in almost all the recent studies. As a specific example, we mention the comparison of two continuous-flow electrolyzers, where an In metal foil electrode was compared with In nanoparticles (100–300 nm) immobilized on a carbon GDL. Seven-fold higher partial current densities towards HCOOH formation were detected in the latter case, compared to the simple indium foil [83].

Fig. 6 summarizes the typical components of a GDE, which includes the GDL, the microporous layer, and the catalyst (possibly together with an ionomer) [78]. The importance of the tri-phasic solid/liquid/gas interface is also highlighted. The effect of GDE structure (e.g., thickness, porosity, and density) on the electrocatalytic properties was extensively studied in fuel cells and water electrolyzers; much less attention has been dedicated to these parameters in the case of flow CO_2 electrolyzers so far. As an exception, optimization of the gas diffusion electrodes consisting of a carbon fiber

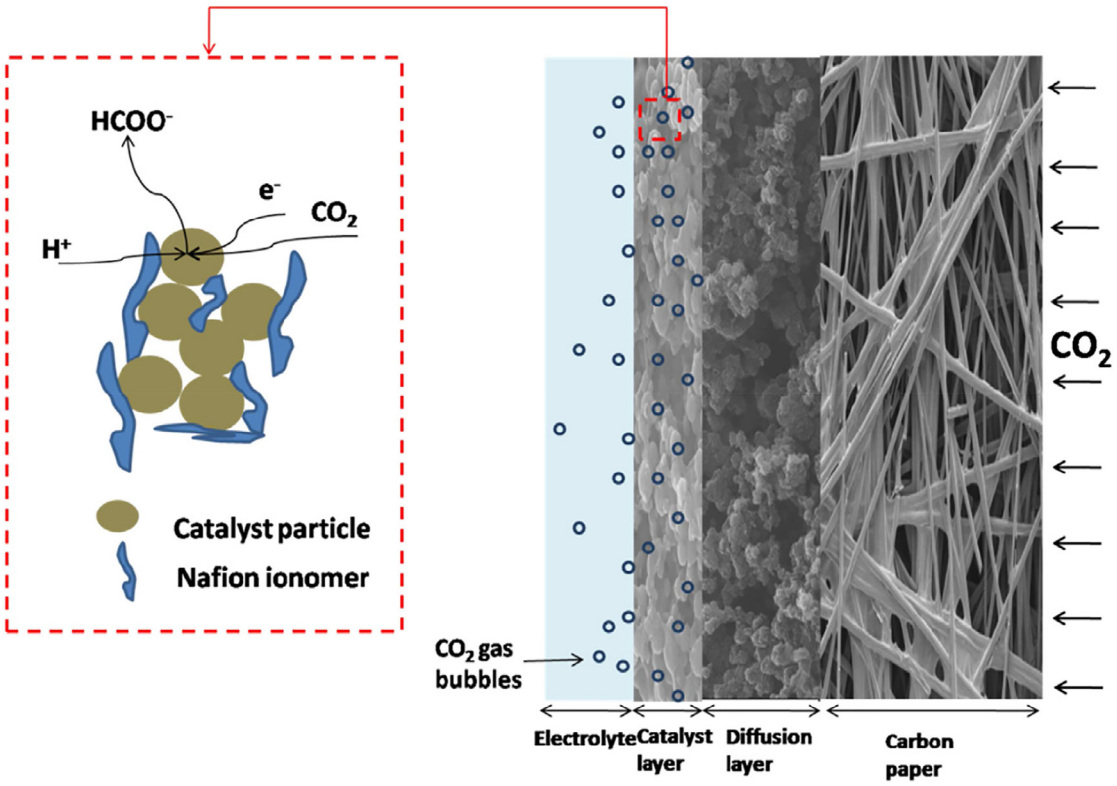

Fig. 6. Schematic composition of a gas diffusion electrode (GDE) and the three-phase interface. Reproduced with permission from ref. [78].

substrate, a microporous layer, and a catalyst layer was performed very recently [84]. The optimized electrode exhibited a higher partial current density for CO production than Sigracet 35BC, a commercially available GDE. Overall, we are convinced that there is a significant opportunity for the rational design of GDEs for further improvement of such devices.

Another very important aspect in the case of flow electrolyzers working with liquid electrolytes is the hydrophobic/hydrophilic properties of the GDL. In the case of fuel cells, an important role of the hydrophobic GDL is the removal of excess water. The case is however different for flow CO_2 electrolyzers: the solution must be kept in contact with the catalyst surface for a sufficiently long time. Proper wetting of the top of the carbon support therefore is a prerequisite, but too much hydrophilicity should also be avoided, because H_2 evolution would be favored in that case. Different ionomers are employed to circumvent the above contradiction, which in turn also contributes to the fixation of the catalyst on the surface of the gas diffusion electrodes (Fig. 6). We also note that controlling the interfacial chemistry between the components of the electrode assembly is of prime importance to ensure high performance and stability at the same time.

3.4. Catalyst immobilization

The technique employed for the catalyst immobilization has a decisive influence on the performance of flow electrolysis setups. The most often used techniques include two steps: first the electrocatalyst is prepared and subsequently, it is transferred to the GDL (or other substrate) or more frequently to the membrane to form the so-called membrane electrode assembly (MEA), via a physical method. We note here that no "standard" catalyst immobilization method exists, but paint- and air-brush techniques are the most common ones. As demonstrated in a recent study, the immobilization technique influences both the measured current values and the product distribution (Fig. 7) [58]. In addition, according to our own experience, the catalyst deposition method affects the stability of the cell as well: channel formation and degradation can be observed if the catalyst is not evenly dispersed, rooted in the uneven distribution of the current flow (see also Fig. 7 for catalyst distribution details).

In situ deposition methods, in which the catalyst is directly formed on the substrate, constitute the other large, but less frequently applied class of immobilization techniques. Electrochemical deposition of different catalysts, exploiting the conductive nature of the carbonaceous GDLs is a particularly promising avenue to form such architectures. The catalyst/GDL structure is thus formed in a single step, and intimate electrical and physical contact between the electrocatalyst and the carbon substrate is ensured. Further, after careful pretreatment of the GDL layer (to tune its hydrophobic/hydrophilic character) not only the top of the GDL is decorated with catalyst (nano)particles, but the inner regions as well. This can lead to increased current values because of the enlarged electrochemically active surface area. A recent study presented the electrodeposition of Sn on carbon fibers thus forming a GDE as a promising

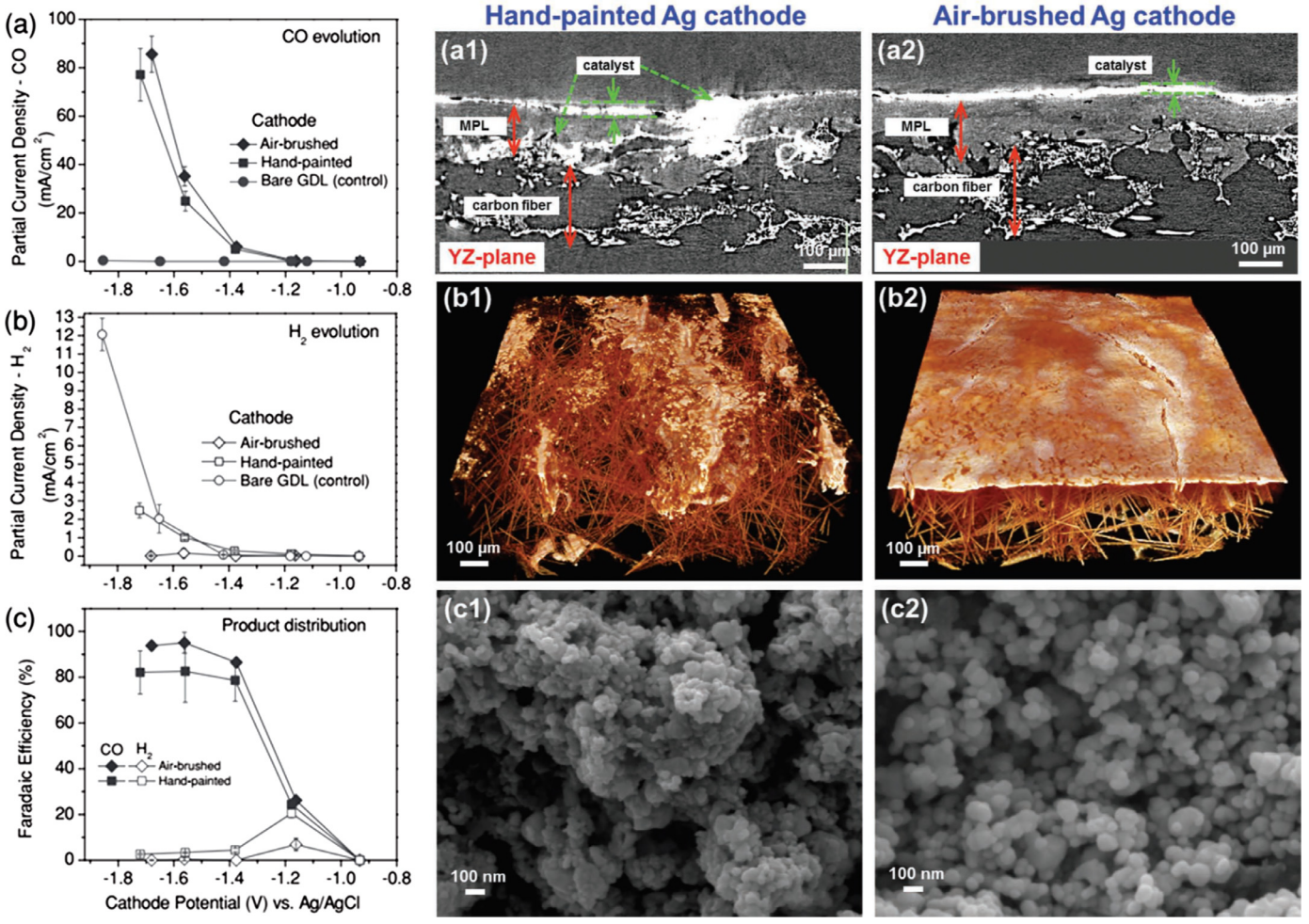

Fig. 7. The effect of the immobilization method on the Faradaic efficiency and specific current density of CO and H_2 formation in a continuous flow electrolyzer with Ag/C cathode. Reproduced with permission from ref. [58].

example [85]. Note however that this approach requires careful optimization of the synthesis circumstances for each catalyst/GDL pair, and is therefore not compatible with rapid screening needs.

One further aspect to consider when immobilizing a catalyst is the use of any binder material (e.g., Nafion™ dispersion). Adding an ionomer to the dispersion of the catalyst before transferring it to the membrane/GDE, influences the subsequently formed catalyst layer. It has a substantial effect on (i) the electroactive surface area of the immobilized catalyst (three dimensional reaction zone) (ii) the ionic (proton) conductivity of the catalyst layer (iii) the hydrophilic/hydrophobic property of the catalyst layer (iv) the interaction (electrical) between the catalyst layer and the membrane. The effect of the relative ionomer content was extensively studied for PEM fuel-cells [86–89]. These works revealed that the cell performance can be enhanced by adding small amount (typically 10–20 wt.%) of the ionomer into the catalyst layer. This results in a large decrease in the ohmic and transport resistance of the layer and extends the active surface area where the electrochemical reaction occurs.

As for the electroreduction of CO_2, the same effect was demonstrated by forming catalyst layers of Sn nanoparticles (100 nm in size) with the same catalyst loading, but by systematically varying the ionomer content [78]. Similarly to the case of the PEM fuel-cells, an initial increase in both the current and the FE was witnessed with the increasing ionomer content, followed by a sharp decrease in the cell performance when the Nafion content was further increased.

3.5. The role of ion-exchange membranes

In those setups that contain an ion-exchange membrane (see Fig. 3), its properties also affect the performance of the cell. The chemical structure, thickness, and the wetting properties all have substantial influence, although their precise contribution have not been fully explored yet. While the clear majority of the studies employ cation exchange membranes, and specifically Nafion™, as the ion-exchange membrane (see some other examples in Fig. 8), there is a considerable scope in tailoring physical-chemical

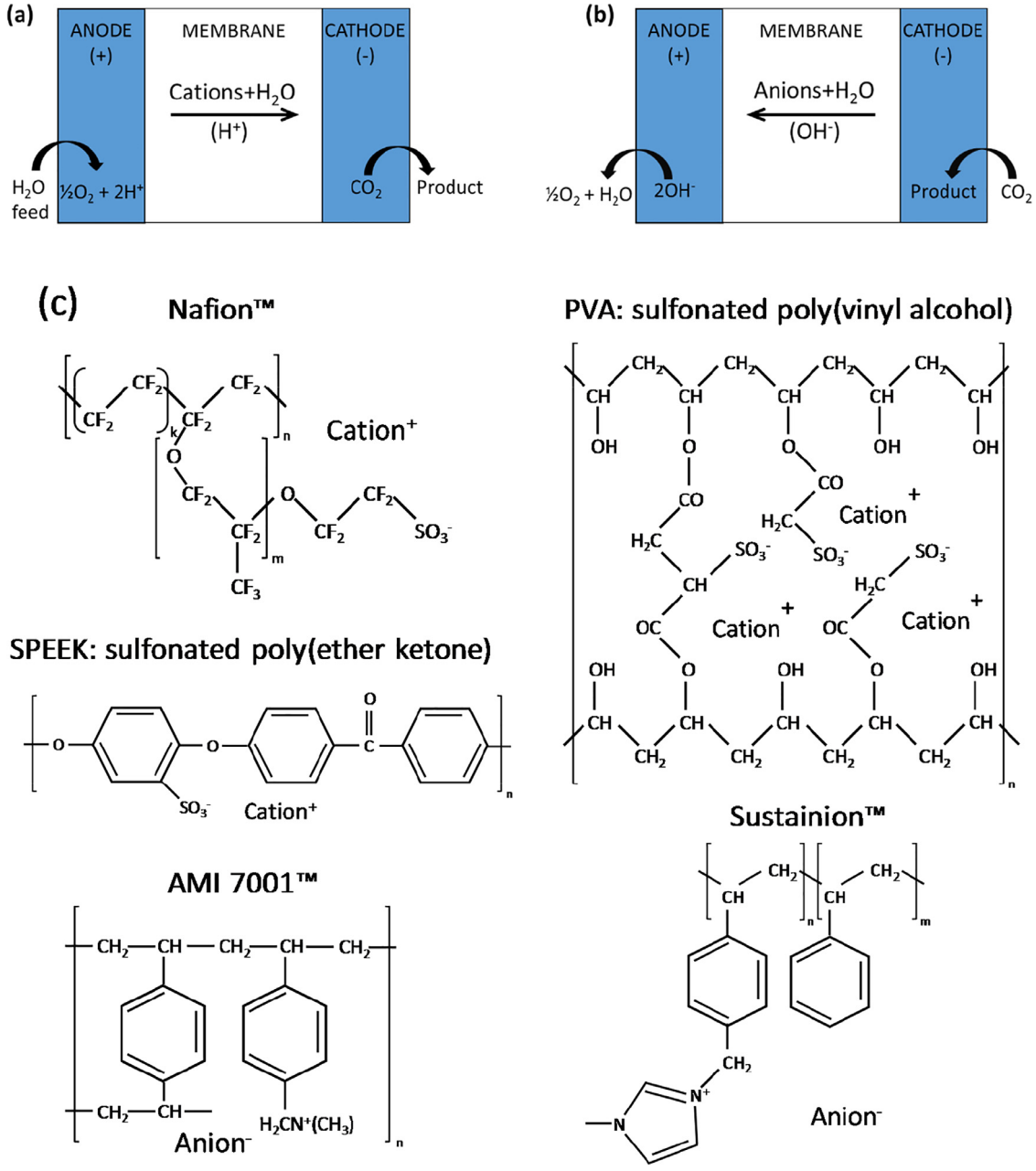

Fig. 8. Illustration of PEM electrolyzers with a cation (a) or anion (b) exchange membrane. (c) Structures of the most common membranes.

properties of the membrane towards CO_2 electroreduction (or even towards specific product formation) [66,90]. Chemical modification of well-known polymers with new organic mediators may open up a new avenue in the future [91,92]. Finally, in addition to chemical factors, durability and pressure handling are two equally important physical attributes to consider.

Four different membranes (Nafion™, SPEEK, alkali-doped PVA, and Amberlyst/SPEEK) were compared in a continuous-flow cell using Pt/C anode and Cu/C cathode for CO_2 reduction [52]. Both the measured current density as well as the relative amounts of the products showed a notable variation as a function of the chemical properties of the membrane. This distinction was rationalized predominantly by the vastly different ionic conductivity of the membranes [52]. In another recent study several chemically different membranes were compared, and an ionic-liquid inspired polymer (anion exchanging Sustainion™) was introduced, providing both high efficiency and stability [93]. For those applications where H_2 formation is to be avoided (e.g., space utilization, see also the Outlook section) the use of anion exchange membranes may help by suppressing proton reduction. This trend was demonstrated when an anion- and cation exchange membranes were compared using a Ag-cathode [94]. Most recently, bipolar membranes have offered enhanced water splitting via steady-state pH gradients and product separation, and these novel materials may be worth exploiting for CO_2 reduction studies as well [95,96]. Finally, we note that product crossover is an important factor to be considered for these membranes from the early development stage.

3.6. The role of the current collectors, bipolar plates, and cell body

The mechanical stability of an electrolyzer is ensured by the cell body, the current collectors (end-plates), and the bipolar plates. As the cell body is a passive element in the setup, the most important requirements to fulfill are chemical inertness and mechanically stability, hence it must not change its shape or dimensions during the electrolysis. This is particularly relevant when the cell operates at high pressure and/or high temperature conditions. The cell body is therefore most frequently made of stainless steel, and its two parts are pressed and held together by several steel screws.

When considering the industrial application of continuous-flow CO_2 electrolyzers, we must distinguish between the microfluidic and the PEM arrangements (see again Fig. 3). While for the first group the scale-out strategy (and therefore the parallel operation of large surface area setups) seems to be favored, the scale-up strategy seems to be the best way of industrial application of PEM CO_2 electrolyzers – very similarly to PEM water electrolyzer and PEM fuel-cells. In this case, several electrocatalyst layers and membranes (MEAs) are coupled in series, separated by bipolar plates, functioning as anode on one side and cathode on the other side (see a typical PEM fuel cell setup in Fig. 9 as an example). The function of these bipolar plates and end-plates is complex: (i) they form the electrodes which are in contact with the catalyst layers, (ii) as the reactants are fed to the catalyst layer through the channels formed in these plates, they are responsible for the reactants supply to the cell active area, and for the proper outlet of the products. Furthermore, they play a significant role in the water and heat management of the cell (most importantly in the case of PEM setups, fed with humidified gases) [98]. To serve this purpose, flow-channels are formed on these plates to increase the surface area, and to help the transport processes [97]. As it was shown for PEM fuel-cells, the different flow-field designs (e.g., straight flow channels, single- or multiple serpentine channels, etc.) have both pros and cons, and therefore this pattern must be always optimized towards the targeted application in the employed setup. The use of current collectors with flow-patterns in continuous-flow CO_2 electrolyzers needs extensive investigations and use of different flow-patterns might contribute to the scale-up and industrialization of this process.

4. Operation

All factors governing the performance on a sub-reactor level were summarized in the previous sections. Now we turn the focus to the operation of the *complete* electrochemical cell, and review parameters that affect the EC CO_2 reduction reaction in the continuous-flow mode. Note that the effects of the discussed parameters are not independent of each other. In fact, their influences are rather complex and convoluted; therefore it is often difficult to carry out studies where only one parameter is varied. Table 2 lists selected examples of continuous-flow CO_2 electroreduction studies from the literature, where the effect of the most important factors is highlighted.

4.1. Feedstock

The first question related to the input flow turns back to the reactor design (see also Fig. 3). It seems that in most studies there is a parallel feed of liquid electrolyte and CO_2 gas; however, there are reports with liquid or gas feed only. Here the reader must be very careful, because certain articles claim solution+gas flow, although when examined closely, only liquid flow (which was previously saturated with CO_2) was deployed. It is also worth noting that all those studies where notably high currents were reported employed *both* gas and solution feed. While the gas feed was almost always pure CO_2 (see discussion later on pressure effects and an exception where Ar/CO_2 mixtures were studied [85]), the composition of the liquid electrolyte varied massively throughout the studies (Table 2). This

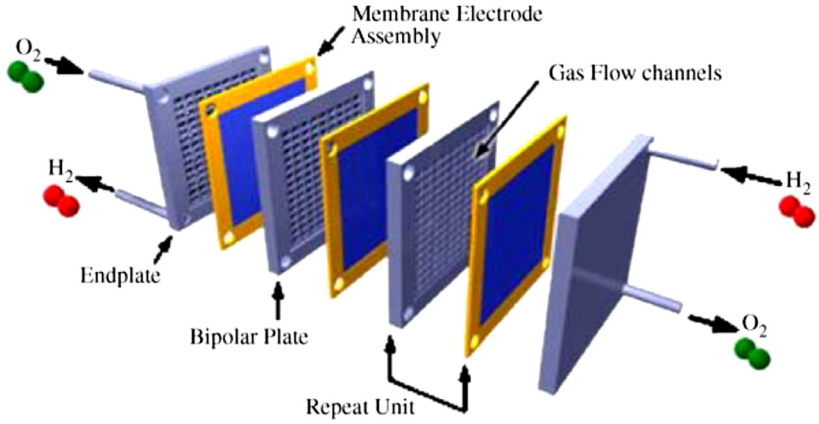

Fig. 9. Stack components of typical fuel cell. Reproduced with permission from ref. [97].

Table 2
The role of operational conditions in the continuous-flow electroreduction of CO_2. The sorting factor was the achieved current density.

Setup	Electroactive material	Electrolyte type	Electrolyte composition	Temperature	Pressure	Current density (mA cm^{-2})	Main Products (FE)	Time	Ref.
Microfluidic	Ag	Solution + CO_2 gas	KCl, KOH, $KHCO_3$, EMIM Cl, Choline Cl	RT	Ambient	440	CO (95+)	n/a	[39]
Microfluidic	Ag	Solution + CO_2 gas	1 M KOH	RT	Ambient	350	CO (95)	7 min	[38]
Microfluidic	Pb	Solution + CO_2 gas	0.5 M K_2SO_4 (0.5 M H_2SO_4)	RT	Ambient	345	Formate (95)	500 min	[37]
PEM	Sn	Solution + CO_2 gas	0.5 M $KHCO_3$ + 2 M KCl	314 K	600 kPa	310	Formate (61)	100 min	[54]
PEM	Sn	Solution + CO_2 gas	0.5 M $KHCO_3$ + 2 M KCl	RT	Ambient	300	Formate (70)	4 h	[55]
Microfluidic	Ag	Solution	1 M KOH	RT	Ambient	280	CO (90)	4 h	[84]
PEM	Ag	Solution + CO_2 gas	0.5 M K_2SO_4 or 0.5 M K_2SO_4:1.0 M $KHCO_3$	333 K, 363 K	24.6 atm	350/275	CO (80)	70 min	[60]
Microfluidic	Ag	Solution + CO_2 gas	1 M KOH	RT	Ambient	250	CO (90)	n/a	[101]
PEM	Sn	Solution	0.1 M $KHCO_3$	RT	Ambient	250	Formate (80–90)	5 h	[102]
PEM	Ag	Solution + CO_2 gas	0.5 M K_2SO_4	333 K	20 atm	225	CO (90)	90 min	[103]
PEM	$La_{1.8}Sr_{0.2}CuO_4$	Solution + CO_2 gas	0.5 M KOH	–	Ambient	180	EtOH (30)	3.5 h	[104]
PEM	Cu	Solution + CO_2 gas	1 M KOH	RT	Ambient	150	CO (57)	4 h	[33]
Microfluidic	Pb	Solution + CO_2 gas	0.5 M K_2SO_4 (0.5 M H_2SO_4)	RT	Ambient	143	Formate (95)	n/a	[74]
PEM	Sn	Solution + CO_2 gas	0.5 M $KHCO_3$ + 0.5 M KCl	RT	120 kPa	130	Formate (86)	10 min	[54]
PEM	Ag	CO_2 gas	–	RT	Ambient	100	CO	250 h	[53]
Microfluidic	Ag	Solution + CO_2 gas	1 M KCl	RT	Ambient	100	CO (80–95)	n/a	[58]
Microfluidic	Sn	Solution + CO_2 gas	0.5 M $KHCO_3$	RT	Ambient	100	Formate (89)	n/a	[35]
PEM	Ag	Solution + CO_2 gas	0.8 M K_2SO_4	343 K	Ambient	100	CO (30–90)	4 h	[59]
PEM	Sn/Cu	Solution + CO_2 gas	0.45 M $KHCO_3$	RT	115 kPa	100	Formate (13–86)	3 h	[71]
Microfluidic	Ag	Solution + CO_2 gas	1 M KOH	RT	Ambient	100	CO (90)	n/a	[61]
PEM	Sn	CO_2 sat. Solution	CO_2 sat. 0.5 M NaOH + 1 M $NaClO_4$	RT	Ambient	97	Formate (58)	10 min	[105]
Microfluidic	Ag	Solution + CO_2 gas	1 M KOH	RT	Ambient	95	CO (90)	n/a	[36]
PEM	Sn	Solution + CO_2 gas	0.45 M $KHCO_3$ + 0.5 M KCl	RT	Ambient	90	Formate (70)	90 min	[82]
Microfluidic	pyrolyzed CN/CNT	Solution + CO_2 gas	1 M KCl	RT	Ambient	90	CO (98)	n/a	[106]
PEM	Ag	Solution	1 M Li^+/Na^+/K^+/Cs^+ /Cl^-/ Br^-/I^-/OH^-	RT	Ambient	80	CO (60–95)	n/a	[100]
PEM	Ag	Solution + CO_2 gas	0.5 M $KHCO_3$	RT	Ambient	80	CO (30–80)	285 min	[107]

variation is quite surprising, considering the prominent role the electrolyte may play in the electrochemical process [39].

The role of the electrolyte, by varying both concentration and chemical makeup, was investigated using a Ag-based gas diffusion electrode as cathode [39]. It was found that anions play a significant role in the process, as reflected in the onset potential for CO formation shifting in the order $OH^- < HCO_3^- < Cl^-$ (Fig. 10A and B). This trend was explained by the interplay of several factors such as pH, conductivity, and, more importantly, specific adsorption of certain anions on the electrode surface. Similar conclusions were drawn for a Sn-based electrolyzer, where OH^-, HCO_3^-, Cl^-, and HSO_4^- anions were studied [99]. The effect of electrolyte anions and cations was further elucidated, by investigating four cations (Na^+, K^+, Rb^+, Cs^+) and four anions (i.e., Cl^-, Br^-, I^-, OH^-) [100]. A major size dependence was observed for the cations, namely an increased CO_2 reduction (and decreased H_2 evolution) activity was detected when larger cations were present in the solution. This trend was rationalized by the better hydration of smaller cations which thus are less likely to adsorb on an electrode surface. The larger cations were thought to adsorb on the cathode repelling H^+ ions from the cathode and stabilizing the "CO_2^-" intermediate on the electrode surface [100].

As for the effect of electrolyte concentration, a monotonic increase in the current density (as well as the energy efficiency) with increasing electrolyte concentration was noted (Fig. 10C and D). Electrochemical impedance spectroscopy (EIS) showed that both the charge transfer resistance (R_{ct}) and the cell resistance (R_{cell}) decreased with increasing KOH concentration [39]. The effect of catholyte concentration (varied in the range: from 0.1 mol dm^{-3} to 2.0 mol dm^{-3}) on product (formate) selectivity was also studied using a tinned copper mesh electrode [54]. An optimal intermediate $KHCO_3$ concentration (0.45 mol dm^{-3}) was found, and rationalized in terms of the competing effects of surface speciation, ionic conductivity, and CO_2 solubility. We note here that CO_2-saturated KOH and $KHCO_3$ solutions are very similar in nature, only the species distribution and the pH being different. As seen in Table 2. there are examples for the addition of an inert electrolyte (e.g., KCl or $NaClO_4$) to such solutions, further improving the electrical (ionic) conductivity without severely affecting the other parameters mentioned above [54,55,82,100]. As a general conclusion, we can state that higher electrolyte concentration leads to higher current densities, unless there is a specific adsorptive interaction with the electrode surface.

Ionic liquids are an emerging class of solvents in CO_2 electroreduction [108]. These materials are special in many aspects, for example they can even stabilize the formed reaction intermediates in CO_2 reduction. Synthetic chemistry allows considerable latitude for tailoring the molecular structure of these liquids, and thereby enhance CO_2 solubility via specific chemical interactions [53,108,109]. The chemistry learned for ionic liquids might be exploited as either surface modifiers or ionomers in membrane electrode assemblies (MEAs) discussed below.

The effect of solution pH is also rather complex and the conclusions cannot be generalized for different electrocatalysts and targeted reduction products. In general, at lower pH values, the formation of H_2 is more favored. However, to form hydrogenated CO_2 reduction products (e.g., formate and methanol), a lower pH is beneficial, while higher pH is suitable for CO formation. The pH effect was studied in a microfluidic reactor, employing a Sn cathode and a Pt black anode [35]. Experiments were carried out at three different pH values, and the cell voltage, the electrode potentials, and the efficiencies (energy and Faradaic) were monitored (Fig. 11). The pH is seen to exert a more prominent effect on the cathode process. At lower pH, the formation of formic acid was favored, both in terms of higher current density and selectivity [35]. This study also calls attention to the importance of having two reference electrodes in the cell, enabling the monitoring of both half-cell processes separately.

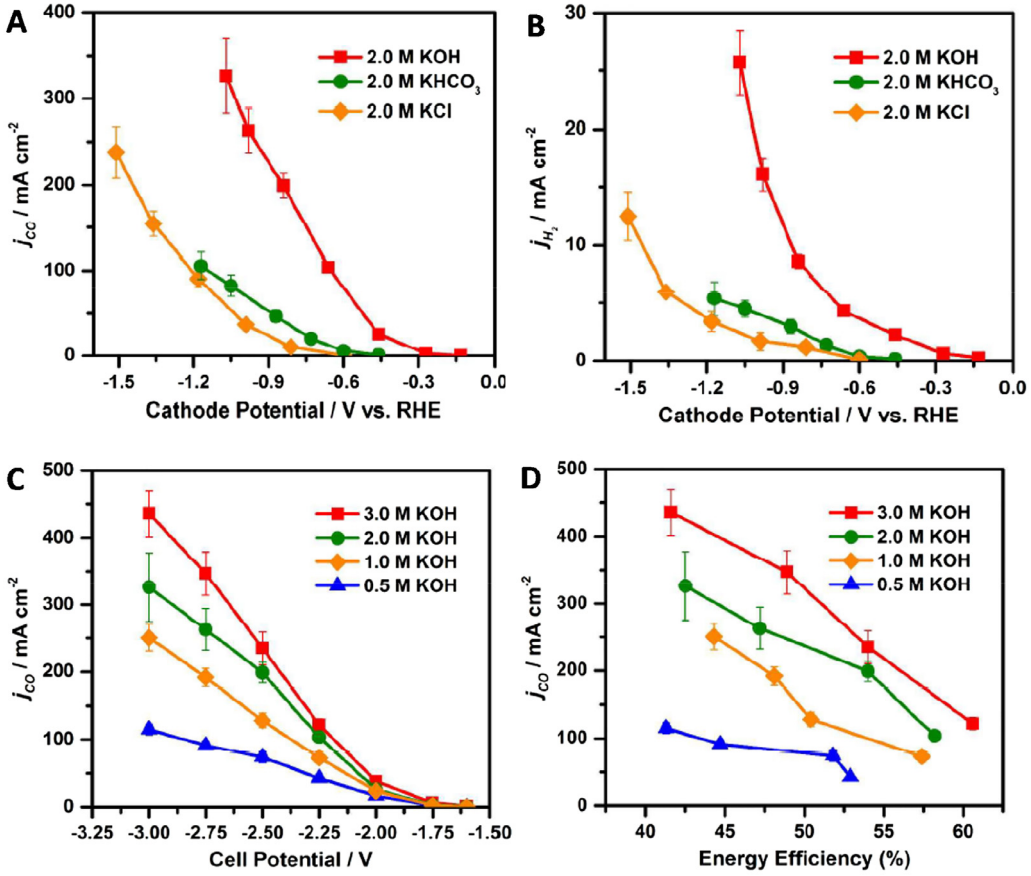

Fig. 10. The effect of electrolyte nature and concentration on the CO_2 reduction current density and energy efficiency in a continuous-flow electrochemical cell. Adapted with permission from ref. [39].

More recently, a dual electrolyte microfluidic reactor was designed, and the effect of using anolyte and catholyte of different pH was systematically studied. A set of electrocatalysts was investigated, and it was concluded that catholyte pH = 2 and anolyte pH = 14 resulted in an optimal cell performance. Furthermore, a three-fold increase was witnessed in the overall performance, compared to the single neutral (pH = 7) electrolyte arrangement [37].

4.2. Liquid/gas flow rate

With the aim of converting large amounts of CO_2, the question occurs instantly: how does the flow rate of the liquid/gas input influence the current density and the Faradaic efficiency (and thus the overall CO_2 conversion process)? Considering the importance of this parameter, it is very surprising that there is no precise definition to meaningfully present the CO_2 flux in the electrolyzer. In almost all the cases, the unit of standard cubic centimeters per minute (sccm) was employed to characterize the gas flow, which equals cm^3/min at standard temperature and pressure. While this unit sufficiently describes the overall gas flow, it gives only very limited information on the actual flux of CO_2 reaching the electrocatalyst surface in the electrolyzer. Consequently, it is very difficult to compare studies performed in different laboratories on electrolyzers of different size. It seems to be a useful exercise to normalize the flow rate with the *electrochemically-active* surface area of the electrode, and/or to the free volume of the cathode compartment of the electrolyzer, thus obtaining the actual flux of CO_2 (see below). In addition, the fact that more often than not,

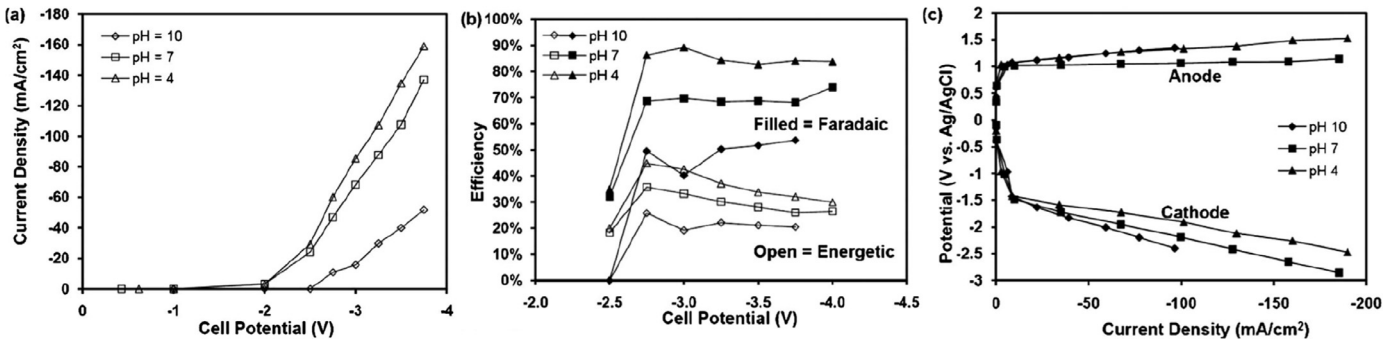

Fig. 11. The effect of pH on the performance of a microfluidic continuous-flow electrolyzer, employing Sn cathode and Pt anode. Adapted with permission from ref. [35].

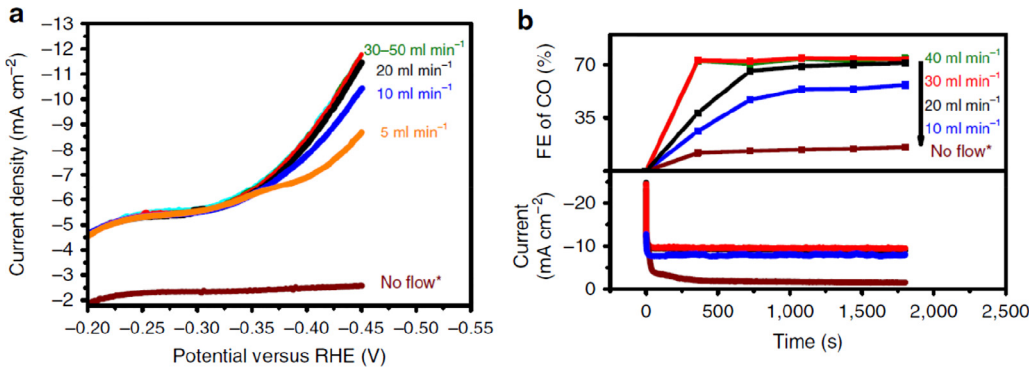

Fig. 12. Effect of CO_2 flow rate on the performance of a batch electrolyzer, but under continuous CO_2 purge. The applied potential was E = −0.4 versus RHE in (b). Reproduced with permission from ref. [31].

pure CO_2 (or solutions with different CO_2 concentrations) is fed to the cathode, implies that the flow rate should be also normalized with respect to the CO_2 content. This exercise was nicely performed in a recent study on Sn-GDE electrodes, where the Ar/CO_2 ratio was systematically varied, while the flow rate was kept constant [85].

In a very recent study, copper hollow fiber electrodes were employed as both the gas diffusion layer and cathode electrocatalyst; and the effect of CO_2 flow rate on the cell performance was studied [31]. As presented in Fig. 12, there is a considerable effect on both the overall current density and the FE for CO generation. The enhancement in FE towards CO as a function of CO_2 flow rate is consistent with a concurrent increase in current density, suggesting that the FE of CO strongly depends on the efficiency of mass transfer of CO_2 to the electrode surface. After reaching a certain flow rate, the achieved steady behavior suggests that most active catalyst sites are involved in the reaction and the kinetically controlled regime was reached [31]. The importance of CO_2 transport in nanostructured electrodes was also demonstrated for electrodeposited Cu nanofoams, where a thickness-dependent selectivity was observed for the formation of formic acid and CO (vis-a-vis hydrogen evolution) [110].

A similar trend was reported for a dual microfluidic reactor, where after reaching a certain threshold, further increase of the flow rate had no effect on cell performance [37]. Over this flow rate, mass transfer rate of CO_2 through the GDE becomes the bottleneck. A higher porosity and smaller thickness of the GDL may help to improve the performance, however, its coherent structure has to be maintained to sustain its mechanical stability and its electronic communication with the current collector.

Besides the achievable current density, product distribution can also be tailored by the flow rate. For example, the effect of flow rate on the H_2/CO ratio was studied in a hybrid PEM/microfluidic reactor, having a Ag cathode and Ru anode [59]. It was demonstrated that by controlling the current density and the CO_2 flow, it was possible to tailor the H_2:CO product ratio between 1:4 and 9:1. Not surprisingly, by limiting the amount of CO_2 reaching the electrode surface, an increase in the H_2:CO ratio was seen. At the same time, this increase in the ratio was not accompanied by any change in the cell voltage or cathode potential [59]. Importantly, after a short induction period, the product ratio was maintained for a relatively long time (5 h). These data suggest that there is considerable scope for tailoring the product ratio, for syngas formation, simply by optimizing the flow rate. Notably, such output can be directly utilized in different chemical processes, for example in the Fischer–Tropsch synthesis.

Finally, we highlight a study where considerable attempt was made to normalize the flow rate, although with the geometrical surface area. Experiments were carried out at three different electrolyte flow (Q) / electrode area (A) ratios and both the amount of the formed products, as well as their distribution varied [50]. Even more interestingly, a Cu electrocatalyst with two different morphologies (Cu plate and Cu_2O derived Cu on carbon support) were compared, and different behavior was seen (Fig. 13). This may be rooted, at least partially, in the different electrochemically-active surface area in the two cases, further highlighting the importance of the suggested normalization protocol (see Section 5).

4.3. Temperature and pressure

As seen in Table 2, there are only few examples where the pressure and temperature were varied from ambient values. The number of systematic studies is even smaller [59,60,103,111], but it seems that higher operating temperatures correlate with higher currents (Fig. 14). This effect however is also complex, because higher temperature leads to lower CO_2 solubility (causing also a change in the pH), but higher diffusion coefficient and reactivity [29]. In these studies the temperature had little effect on the selectivity [103], but this is likely to vary a lot depending on the electrocatalyst. Over a certain temperature, current increase is associated with a decrease in FE of CO_2 conversion, and thus increased H_2 evolution [60]. Our own, currently ongoing work suggests that lower temperatures (e.g., 3 °C) promote ethylene formation over methane for copper-based cathodes in a GDL-configuration. Considering the complex effects of temperature, many more studies are needed in this direction with in situ monitoring of the temperature in the electrolyzer, which is not trivial.

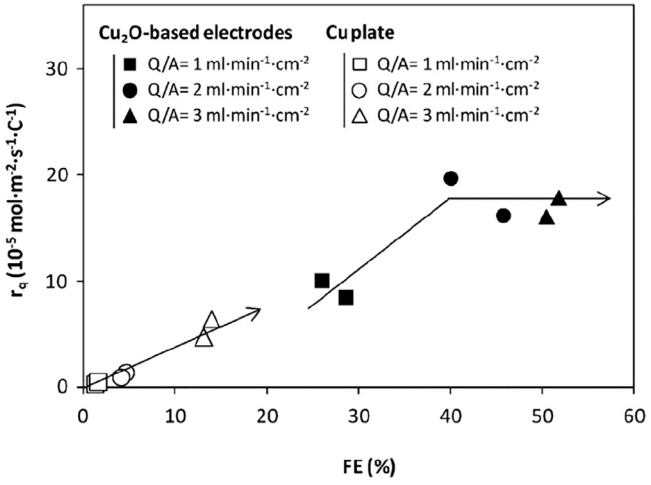

Fig. 13. Comparison of the product formation rate and FE for two different electrodes at three different surface area normalized flow rates. Reproduced with permission from ref. [50].

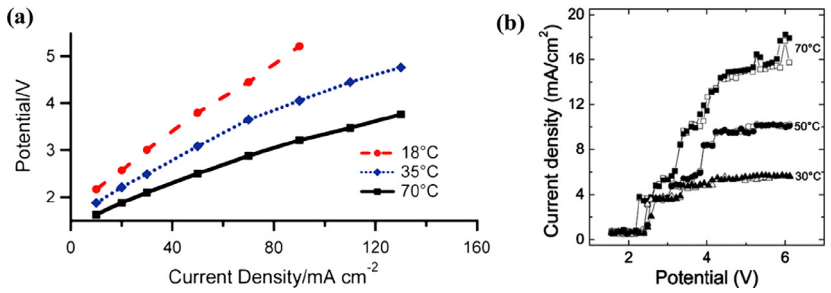

Fig. 14. The effect of temperature on the operation of two CO_2 electrolyzers with Ag (a) and Cu felt (b) cathode. Reproduced with permission from refs. [59,111].

The effect of pressure is even less studied although increased pressure: (i) increases the solubility of CO_2 according to Henry's law; (ii) enables work at higher temperatures; (iii) makes it easier to store, or to react the products (e.g., syngas) further to value-added products. The pressure was gradually increased in a combined PEM + microfluidic reactor setup (see Fig. 3A) from atmospheric to 20 atm. A five-fold increase in FE towards CO evolution was seen both at room temperature and at 60 °C (Fig. 15) [60].

4.4. Effect of the applied potential/voltage

The potential/current dependent product distribution has been extensively studied in batch reactors. Much less is known about continuous-flow setups, but a comprehensive study using a PEM electrolyzer (Cu cathode, Pt anode) was able to detect as many as 16 reaction products (Fig. 16). At low overpotentials, only hydrogen, CO, and formate were observed, with the dominance of hydrogen formation at very low overpotentials. As the overpotential increased, cumulative FE of CO_2 reduction products increased versus H_2 formation. First hydrocarbons (methane and ethane) were formed, while at even higher voltages, C2–C3 products were produced [19].

The effect of the applied potential is less complex in those cases where only one product (e.g., formate, CO) is formed [38,112,113]. Note however that H_2 evolution is a competing reaction even in these instances. As the external driving force (potential/voltage) is increased, this latter becomes more and more prominent, leading to a volcano-type plot for the Faradaic efficiency of the product with the applied potential. One hand, this is disadvantageous, since the production rate of the intended product cannot be increased while maintaining a high energy-efficiency. On the other hand, this gives the opportunity to form specific product mixtures. For example, using a silver containing GDE cathode, the H_2/CO ratio was tuned to form readily processable syngas simply by varying the applied current density (and hence the potential) [59].

4.5. Timescale of the experiments

As seen in Table 2, the timeframe of the electrolysis experiments span a few minutes to a few hours. Interestingly, in many cases, no stationary electrolysis was performed, and the current values were gathered from linear sweep voltammetry (LSV) experiments. There are only a few studies where the product distribution was reported as a function of time. This information would be crucially important in assessing the stability of the electrocatalyst and the entire electrolyzer assembly. For example, the H_2/CO ratio was monitored during a galvanostatic experiment (Fig. 17), using a silver GDE. The monotonic increase in the H_2 evolution ratio (and the decrease of FE_{co}) was rationalized by alteration of the electrode, in particular increased wetting of the GDL [103]. A recent study, employing a solid catholyte and an anion-exchange membrane showed stable selectivity and cell voltage over 250 hours of operation at 100 mA cm^{-2} [53].

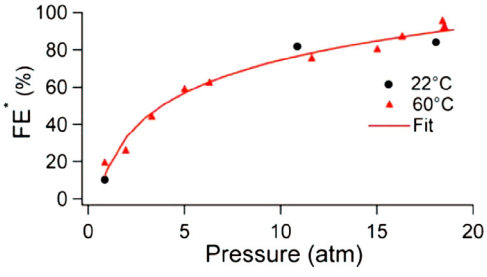

Fig. 15. The effect of pressure on the FE value for a combined PEM + microfluidic CO_2 electrolyzer with a Ag GDE cathode. Reproduced with permission from ref. [60].

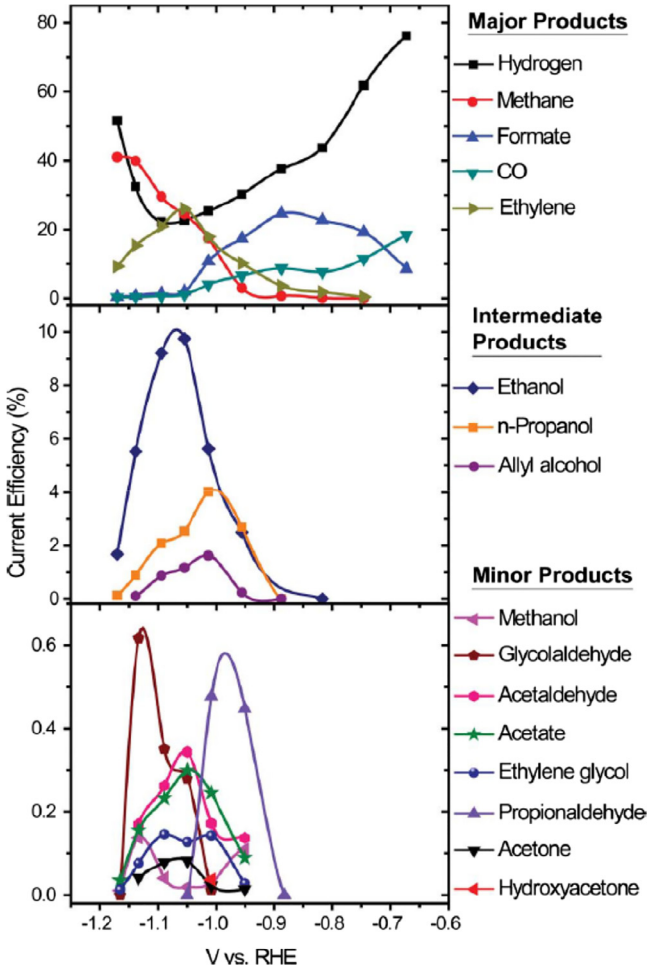

Fig. 16. Effect of applied voltage on the product distribution in a continuous-flow CO_2 electrolyzer with a Cu cathode. Adapted with permission from ref. [19].

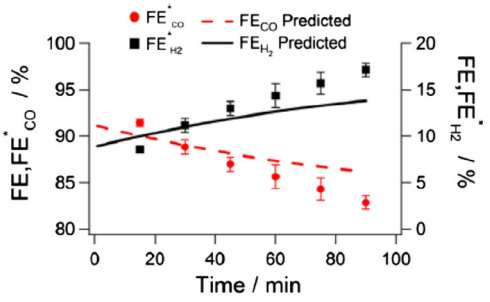

Fig. 17. Alteration of the product selectivity with time in a pressurized PEM electrolyzer with a silver cathode. Reproduced with permission from ref. [103].

5. How to benchmark a CO_2 electrolyzer correctly?

As data-mining turns into a major component of every research project, it is now more important than ever to report experimental data (and the drawn conclusions) in a manner where comparisons from laboratory to laboratory can be easily made. According to lessons learned from allied R&D fields (most importantly fuel cells and electrochemical water electrolysis), setting up a proper benchmarking protocol leads to a more coherent knowledge of these systems, and consequently to an accelerated development of these fields [114–118]. Such a protocol should include characterization of both the electrochemical cell-forming components separately as well as the complete cell itself, via a set of systematic studies. We suggest the following benchmarking experiments to be carried out and a list of figures-of-merit to report, as a framework for testing a new electrolyzer setup. Table 3 briefly summarizes these items, and each of them is further elaborated in what follows.

Reporting the exact details of the cell is of prime importance. This should cover the dimensions of the cell components, their physical and chemical properties (e.g., membrane and GDL type and thickness, chemical composition, pretreatment method), and the degree of compression. We reiterate our earlier point, that without this information, the flow rate of the electrolyte (or the gas)—which is usually provided in units such as sccm or ml/min—gives only very limited information on the retention time of CO_2 in the cell. The flow rate of the electrolyte therefore should be always normalized by either the free volume of the half-cell or with respect to the electrochemically-active surface area of the electrode (or both).

5.1. Pre-operational characterization

The electrocatalyst is the core component of any electrochemical setup, therefore its comprehensive physical and chemical characterization must be the first step of every experimental work. These

Table 3
Proposed benchmarking protocol for continuous-flow CO_2 electrolyzers.

Characterization method	*Requirements*	*Data to report*	
Physical and chemical characterization methods (XRD, XPS, TEM, SEM, EDS, Contact angle, and surface area measurements, etc.)	Multiple scale analysis has to be performed both for the electrocatalyst and the support.	Chemical composition, size distribution, shape, dominant crystal orientation, surface properties	**PRE operation**
Cyclic voltammetry and linear sweep voltammetry of the individual electrodes. Measurement of Tafel-plots	No Faraday process shall occur during CV, reference electrode is needed. Both separately for the two electrodes, and before operation inside the cell. IR-compensation shall be carried out	Electrochemically active surface area, onset potential value at a given current density.	
Electrochemical impedance spectroscopy	Multiple voltage values shall be used.	R_s, R_{ct}, C	
Linear sweep voltammetry	Multiple scan rates. Several subsequent scans, till the stationary behaviour is reached. Comparison of measurements with and without CO_2 shall be carried out, with solutions of the same pH.	LSV curves, current density normalized to both geometric and electrochemically active surface area. Onset potential value at a *given current density*.	**Operation**
Stationary electrolysis (chronoamperometry/chronopotentiometry) coupled with product analysis	Online analyis of both gas and liquid phase products. Measure on multiple current/voltage values (at least 5).	Faradaic efficiencies for ALL products, including H_2 (for all current/voltage values).	
Long term stationary electrolysis (chronoamperometry/chronopotentiometry) coupled with product analysis	Online analyis of both gas and liquid phase products after selected time periods.	Faradaic efficiencies for ALL products, including H_2 (for all current/voltage values) with respect to the elapsed time.	
Electrochemical impedance spectroscopy	Multiple voltage values shall be used.	R_s, R_{ct}, C	**POST operation**
Cyclic voltammetry and linear sweep voltammetry of the individual electrodes. Measurement of Tafel-plots	The same measurements as before operation both inside and outside the cell	Electrochemically active surface area	
Physical and chemical characterization methods (XRD, XPS, TEM, SEM, EDS, Contact angle, and surface area measurements, etc.)	The same measurements as before operation	Chemical composition, size distribution, shape, dominant crystal orientation, surface properties	

	Data to report
Paramaters related to the operation of the electrolyzer	pH, temperature, pressure, electrolyte concentration, surface area/free volume normalized flow rate
Parameters describing the cell setup	Cell configuration and size, properties and dimensions of the individual components (e.g., membrane and GDL thickness), catalyst loading

studies must involve physical, chemical, and surface characterization via different spectroscopic techniques (FT-IR, Raman Spectroscopy), electron microscopy (TEM, SEM), elemental composition analyses (EDX, XRF), surface composition and functional groups analysis (XPS) and crystal phase determination (XRD). Similar characterization of the supporting layer (GDL) must be also performed, supplemented with the characterization of its pore structure (e.g., N_2 adsorption/desorption).

Although the catalyst morphology is one of the most important factors after the chemical composition, often little information could be found in the different articles. We recommend multi-level analysis to be performed before and after immobilizing the catalyst on the substrate, revealing crystallite size, crystallinity of the material, degree of aggregation, and surface properties of the particles. The geometric surface area of the immobilized catalyst can be estimated from the recorded microscopic images, but it must be kept in mind that the electrochemically-active surface area can immensely differ from this value. Therefore this latter parameter has to be calculated from EIS measurements, or by simply recording cyclic voltammograms in a potential window where no Faradaic process interferes [119]. For certain electrocatalysts, the use of model redox active compounds can also be useful.

The activity of an electrocatalyst is most usually characterized by recording linear sweep or cyclic voltammograms. As these are non-stationary measurements (even at low polarization rates), the values of derived kinetic parameters from these, must be treated with caution. Recording of polarization curves provides complementary data. In this case, the stationary potential is recorded at different current densities (spanning several orders of magnitude), and then plotted versus the logarithm of the current densities to afford Tafel plots (Fig. 18). The linear region of the curve is fitted to give the Tafel-slope, which – together with the onset potential of the process – is the most important parameter describing the electrocatalyst.

By performing LSV measurements for the single electrodes in a classical three-electrode electrochemical cell and in the assembled electrolyzer under otherwise identical circumstances (electrolyte concentration, pH, temperature etc.), the effect of the cell construction method (hot pressing, mechanical fixation, etc.) on the catalyst properties can be studied directly. EIS measurements are very useful at this early stage of investigating the cell, as they can reveal any additional resistances (R_s, R_{ct}), arising from failure of the cell assembly and leading to severe losses due to IR-drops in the system. Note, that during electrolysis, as a current (I) is driven between the working and the counter electrode, a potential drop (IR) develops in the setup; originating from the resistance of the cell constituents, the electrolyte, and the membrane. In a three-electrode electrochemical setup, the potential of the working electrode is measured against a stable reference electrode. Although these electrodes are placed very close to each other, some portion of this potential drop is still present between them, which is caused by the so called uncompensated resistance (R_u).The IR_u-drop is dictated by the cell geometry and is dependent on the applied current and its presence leads to distortion of the electrochemical measurements [78]. To secure reliable data on the catalyst activity, the measured potentials must be always corrected for the value of this uncompensated potential drop. For this purpose, the uncompensated resistance has to be measured, which is typically done by either EIS or by the current-interruption technique [121,122]. Overall, the discrepancy between actual and applied voltage requires the use of IR compensation to get reproducible data that is comparable between different laboratories for the various cells, especially those operating at high current densities.

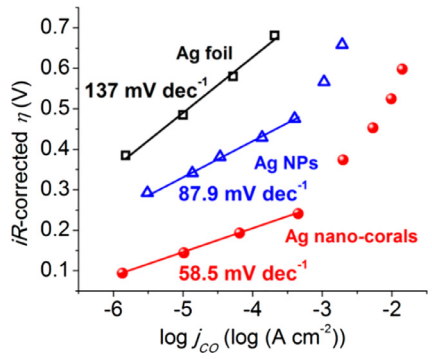

Fig. 18. Tafel plot of different Ag electrocatalysts in a 0.1 M $KHCO_3$ solution purged with CO_2. Reproduced with permission from ref. [120].

5.2. In operando characterization

The most important part of these studies is the investigation of the assembled flow cell during operation. To study the kinetics of CO_2 reduction in the given setup, LSV measurements should be carried out at multiple scan rates. Note that measurements at the first sweep rate must be repeated until steady-state electrochemical behavior is reached. Information gathered from the first cycles can often be misleading, because the measured current can originate from multiple sources, including the reduction of the electrode support or the electrocatalyst itself—as it was observed for the case of Cu_2O derived Cu catalysts [20]. The LSV curves must be always normalized to the geometric surface area and/or to the electrochemically active surface area of the cathode. Comparison of such data to results measured with chemically-equivalent, but different sized catalyst particles can help to understand different size effects beyond the trivial increased surface area/volume ratio. Here we refer to the discussion on the importance of having one or more reference electrodes in the cell (see Fig. 3).

The estimation of the onset potential of a process is always a difficult question. Some researchers derive this value graphically from the LSV curves, while others give the potential value at which the current reaches a certain threshold value. Consequently, the comparison of these data is difficult and often misleading. To avoid confusion, we suggest 1 and 10 mA cm^{-2} as a benchmarking current density (note the similarities with solar powered water oxidation and H_2 evolution) [118]. The LSV measurements serve as a decent guide for choosing the proper potential/current region, where CO_2 reduction studies have practical relevance. Subsequently performed stationary measurements, either at constant current or constant potential/voltage give real insights into the performance of a given setup. These time-dependent experiments must be coupled with in situ product analysis, both for the liquid and the gas phases, since these are better tools for determining the onset voltage (potential) than just using LSV curves.

Designing a proper product-detection setup, however is not straightforward, because there is no single analytical method which can characterize both quantitatively and qualitatively all reduction products generated from CO_2. First, for the analysis of the gas and liquid phase products, we generally need different analysis tools. An online sampling system should be connected to a gas chromatograph (for gas phase analyses) and sealed to avoid any leakage. We highlight a recent development, the barrier ionization discharge (BID) detector, which is universal with greater sensitivity than both the thermal conductivity- (TCD), and flame ionization detectors (FID). Consequently, there is no need for two different detectors to measure H_2 gas and the CO_2 derived products [123].

Analysis of the liquid phase is a little more complicated, because the electrolyte ions must be either removed for the most sensitive GC–MS analysis, or higher sample concentrations are needed for NMR analysis. The performance of the NMR analysis, however, can be improved by special cell design with high surface area working electrode and very low electrolyte volume [124]. Differential

electrochemical mass spectrometry (DEMS) is an effective tool for the real-time detection of electrochemical reduction products, however, the interpretation of the results can be complicated for a reaction which gives a mixture of different products [125]. For example, DEMS cannot be used for detection of CO, because CO_2 gives the same ionization fragments. The quantitative detection of formic acid, because of its deprotonation, is challenging by GC and DEMS as well. The amount of formate can be reliably quantified by ion chromatography. By this technique, however, other solution compounds (e.g. different alcohols) cannot be analyzed [126]. It is therefore of utmost importance to follow the reaction with different instrumental techniques, and to account for all the charge passed during the electrolysis.

It is recommended to clearly state in every manuscript: (i) detection limit for the employed analytical instrument and (ii) the partial current density for the observed product at the onset voltage. We emphasize that because of the frequent use of carbon-based catalyst supports, studies with ^{13}C labeled CO_2 should be performed to clarify the origin of the carbon-containing products. Finally, we note that the selected analytical methods have to be compatible with the electrolyzer setup, possibly limiting the application of certain (otherwise promising) techniques.

The Faradaic efficiency (FE) for all the formed compounds as well as the overall FE has to be reported. Note that FE as defined is strictly the ratio of the charge consumed on a given process and the passed total charge. Some authors—without analyzing the liquid or the gas phase products—mistakenly and misleadingly refer to the ratio of the given product amount and the detected total amount of all the products as the Faradaic efficiency. Similarly, H_2 is also a product (although not CO_2-derived), therefore must be taken into account for these calculations.

The operation of the electrolyzer must be also characterized on a longer timescale. Therefore, the above listed measurements—or at least those which were promising in the sense of current density and product distribution —has to be conducted for several days, while the product distribution is traced after regular time periods. Keep in mind that water electrolyzer cells, working on very similar principles and built from almost identical materials have a reported lifetime in the range of 10,000 h [127], and similarly long lifetimes are required for CO_2 electrolyzers in practical applications.

5.3. Post-operational characterization

After the long-term operation, degradation of the electrochemical cell must be investigated at every level, by repeating the same measurements as before operation, in the reversed order. Thus, an EIS measurement of the cell can reveal corrosion of the cell constituents, while change in the onset potential (derived from LSV measurements) can indicate chemical change of the catalyst. After disassembling the cell, the catalysts must be characterized separately with the formerly used experimental techniques, revealing changes in the catalyst particle size, aggregation, composition, and in the structure of the membrane or the GDL, etc. [128].

5.4. Most important metrics to report

Talking about the efficiency of the cell, one must distinguish among current-, electrical-, and energy efficiency. The current efficiency (or Faradaic efficiency, $\varepsilon_{Faradaic}$) of the process is a direct relation between the number of electrons consumed in a given electrode process and the total amount of the charge passed during the electrolysis. Energy efficiency of a given cell is somewhat more complex concept, as it is not only influenced by the thermodynamics and kinetics of the electrode processes, but electrical parameters of the cell as well. The measurement conditions and heat exchange efficacy during the process may also be important parameters. These

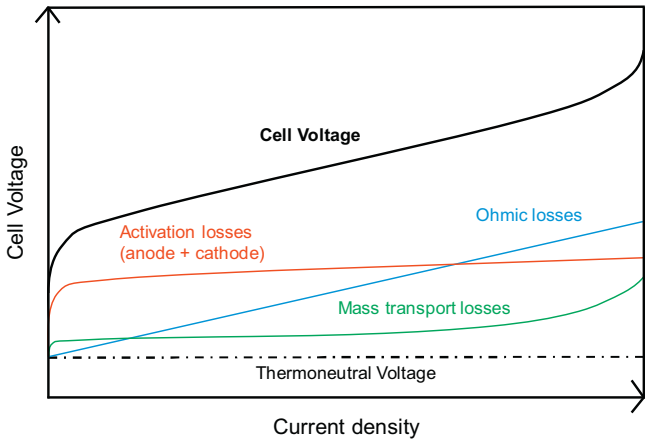

Fig. 19. Different loss-mechanisms potentially affecting the performance of an electrolyzer.

can be defined in different ways, and therefore are a common source of confusion [129].

The most commonly applied, and most straightforward definition is the voltage efficiency of the cell, which gives a good approximation on its operation. This is calculated as the ratio of the thermodynamic voltage needed to drive the given electrochemical process (given by the redox potential of the half-reactions) and the total voltage applied to the electrolysis cell (V_{cell}). Beyond the thermodynamic requirements of the reaction, this latter value is dictated by different energy losses, related to the catalysts (anodic and cathodic overpotential, η_i), to mass-transport, and to the cell itself (IR-drop). Fig. 19 summarizes the most common mechanisms, which lead to an increased cell voltage. Note that the shape of the curves may also be useful for diagnostic purposes when an electrolyzer fails. In addition, these factors can be separated by the above described benchmarking protocol, thus uncovering future development avenues [130].

The above-mentioned efficiency units alone, however, are of low industrial relevance. To give an exact measure on its operation, the energy efficiency of the cell must be calculated during long-term operation. The energy efficiency is most commonly calculated as the product of the voltage- and Faradaic-efficiencies [15]. This is only true, however, if only one single product is formed. If this is not the case (i.e., multiple products are formed in parallel), the individual redox potentials (e.g., $E^{\circ}_{CO2/CH4}$) have to be taken into consideration Eq. (2).

$$V_{cell} = E^0_{anode} - E^0_{cathode} + \sum_i \eta_i + IR_{cell} \tag{1}$$

$$\varepsilon_{energy} = \frac{\sum_i \left(E^0_{anode,i} - E^0_{cathode,i}\right) \times \varepsilon_{Faradaic,i}}{V_{cell}} \tag{2}$$

The energy efficiency can be also defined as the energy content ($E_{content}$) of the given product over the electrical energy consumed during electrolysis, where t is the time of electrolysis to form unity amount of the product. The chemical energy of the produced molecules can be expressed by their Gibbs free energy per mole (ΔG_0). In some articles, the heat of combustion, or enthalpy, has been used to represent the energy content:

$$\varepsilon_{energy} = \frac{E_{content}}{E_{input}} = \frac{E_{content}}{V_{cell} \times I_{cell} \times t} \tag{3}$$

6. Photoelectrochemical reduction of CO_2 in continuous-flow

As a possible alternative on a longer horizon, we would like to briefly mention a few examples of continuous flow

photoelectrochemical (PEC) cells, demonstrated in CO_2 conversion. Historically, PEC solar fuel generation was predominantly focused on water splitting (H_2 evolution), and much less attention was paid to CO_2 reduction, mainly because of kinetic constraints [131]. In direct PEC CO_2 reduction, upon excitation of an electron from the valence band to the conduction band (by UV or visible light irradiation) of a p-type semiconductor (SC) the separated photoelectrons are driven to the surface of the SC and react with CO_2 (or a redox mediator/co-catalyst present either on the surface or in the solution). The CO_2-reducing ability of the photo-electrocatalyst is dictated by the position of the conduction band (CB) edge: it has to be at a more negative potential than the targeted CO_2 reduction reaction. In such a procedure, it is possible to reduce CO_2 *at less negative* potential relative to the thermodynamic potential (vs. electrochemical reduction). The indirect PEC approach is also possible, where an n-type semiconductor photoanode is employed, and CO_2 reduction takes place at the cathode in the dark [132]. By employing either PEC approach, the necessary energy input (cell voltage) can be decreased by the photopotential, which is dictated by the CB edge of the SC photocathode and the redox potential of the CO_2 reduction process (or the VB edge of the photoanode and the water oxidation potential, for the indirect approach).

To enhance the current densities to a level which makes practical significance, however, photoelectrodes with large specific surface area are needed. This necessitates the use of nanostructured photoelectrodes, which is a surprisingly unexplored area, in fact, the long-standing theory of PEC builds on thick electrode films (with film thickness of over several micrometers) [133]. To efficiently drive CO_2 reduction reactions, these carriers need to reach the photoelectrodes interfaces at the electrolyte and at the back contact. Therefore it will be very important to understand the effect of nanostructuring on carrier generation and collection, surface recombination, and on the size of space charge layers [134].

There are only a few examples in the literature, which at least demonstrate the concept of continuous-flow PEC CO_2 conversion. In a recent proof-of-concept study, hybrid CuO/Cu_2O nanorod arrays were incorporated as the photocathode in a new continuous-flow design [68]. The performance of the photocathode was compared to a conventional two-compartment batch type PEC cell. The primary products were alcohols, with a yield which was ~6 times higher than the batch design, and significantly enough, also showed longer-chain alcohol products up to C2–C3 (ethanol and isopropanol). The high surface area-to-volume ratio resulting from the narrow reaction channels resulted in an enhance photocurrent density and Faradaic efficiency.

Even more recently, NASA researchers reported a PEC conversion device, operated at room temperature and ambient pressure with only ultraviolet radiation [135]. They used a nanocomposite electrode which combines a photocatalyst and an electrocatalyst, capable of reducing gaseous CO_2 to methane without the need of external electricity input. Considering the typical solar flux, the achievable current densities are typically lower for these cells (~10 mA cm^{-2}) compared to the electrolyzers presented earlier. In addition, long term stability is an addition hurdle to face, therefore stability tests are even more important in these instances. In other instances, the indirect approach was employed, where the oxidation half reaction took place on a photoexcited n-type semiconductor (specifically, TiO_2). As shown in Fig. 20, the overall cell design is very similar to the conventional PEM electrolyzers, except that the anode is irradiated [132,136]. The principal benefit of this setup is that all the knowledge gathered for the cathode reaction (CO_2 conversion) can be implemented, while the solar energy input is harnessed.

In the case of PEC cells, the photon to product conversion efficiency is defined as the output power, namely, the product of voltage, partial current densities, and Faradaic efficiency for the formation of different products, divided by the denominator, namely, the solar energy input from sunlight:

$$\eta_{PEC} = \frac{j_{photo} \times \sum_i (V_{redox,i} - V_{bias}) \times \varepsilon_{Faradaic,i}}{P_{light}} \quad (4)$$

where j_{photo} is the photocurrent density (mA cm^{-2}) normalized to the illuminated electrode area, V_{redox} is the thermodynamic potential of the given process, V_{bias} is the applied voltage, $\varepsilon_{Faradaic,i}$ are the partial Faradaic efficiencies for the different products, and P_{light} is the power of the incident illumination [137,138].

Alternatively, Eq. (5) uses the chemical energy of the products formed divided by the solar energy input from sunlight incident on the electrode. In this expression, the nominator is directly related to the formation rate of a given product, establishing a direct relation to product analysis during the measurements. Note that this definition is similar to that conventionally used for solar to hydrogen (STH) conversion [139], and is only applicable if no external bias is employed (i.e., at short circuit conditions).

$$\eta_{PEC} = \frac{\sum_i \nu_i \times \Delta G_i}{P_{light} \times A} \quad (5)$$

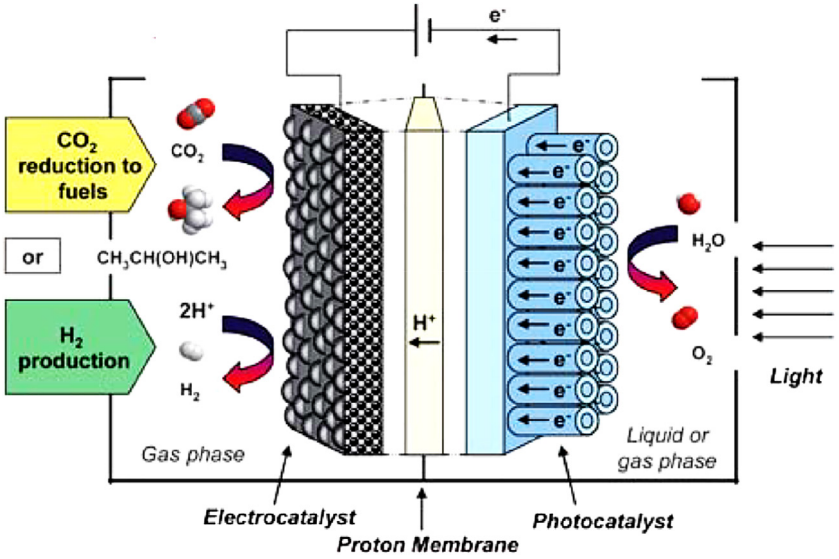

Fig. 20. Schematic illustration of the indirect PEC approach with a PEM cell. Reproduced with permission from ref. [136].

where v_i is the formation rate of a given product (mmol s^{-1}), ΔG_i is the Gibbs free energy per mole of a given product (J mol^{-1}), P_{total} is the incident illumination power density (mW cm^{-2}), and A is the illuminated electrode area (cm^2).

7. Summary and outlook

As demonstrated in this review article, multiple parameters have to be optimized simultaneously to efficiently perform continuous-flow electroreduction of CO_2. Some of them are well understood, while others still need to be carefully studied. The effects of high pressure and temperature are of particular interest to achieve reasonable current density and selectivity. These parameters will also affect the surface of the catalysts [140], which is another factor to be studied in continuous-flow cells. Computational modeling can contribute to the rational design of electrolyzer configuration. In this vein, the reactor performance can be numerically simulated to unravel the influence of flow rate and channel geometry on CO_2 conversion and consumption rate. Similarly, recent advances in 3D printing allows rapid prototyping of different cell geometries and thus will be a powerful tool in the hand of electrochemists [141]. Furthermore, we believe that successful studies in vapor phase will open up the opportunity to use industrial exhaust fume (rich in both CO_2 and H_2O) directly as feedstock for solar fuel generation. Accordingly, different model gases containing typical impurities should be studied in the future.

As for future development avenues, we would like to emphasize two directions. One is coming from the materials perspective: the need for intricate architectures where the elements of the GDE are simultaneously optimized. As shown in Sections 3.3–3.5, rationally designed interfaces are required for efficient CO_2 conversion. In this endeavor, the cooperation of chemists, materials scientists, and engineers is highly recommended. The second R&D path is rooted in the fact that the anode reaction was oxygen evolution (water oxidation, OER) in almost all the presented studies. In such cases the formed oxygen is considered as a non-harmful by-product, and is simply let to the atmosphere without using it for any purpose. We also note that OER as the anode process can be important in Space applications, namely as a root for the recovery of O_2 from CO_2. With the interest of deep space exploration (i.e., possible prolonged missions to Mars), it is of high importance to improve such key enabling technologies. As for terrestrial applications, the formed oxygen can be compressed and sold, but driving a more beneficial electrochemical procedure on the anode could be a value-added approach. In this manner, CO_2 electrolyzers could be easily integrated in other industrial processes, in which the main product is formed on the anode.

There are several candidates, for example, using the oxidation of organic pollutants on the anode, which is a kinetically-facile reaction. Thus the electrolyzer can be employed as both CO_2 converter and water purifier (i.e., wastewater treatment with a net zero CO_2 emission) adding value to the overall process [142]. This can be envisioned by either directly oxidizing the organic pollutants, or indirectly, by generating ozone on the anode. This concept is well-known for water electrolyzers, in which hydrogen is produced on the cathode, while oxidation of water pollutant occurs on the anode [143]. Chlorine (Cl_2) evolution is another technologically relevant reaction, which might be worth coupling with CO_2 reduction (also called chlor-syngas process, see Fig. 21) [144]. Importantly, the redox potential of chloride oxidation matches with that for the water oxidation; therefore, this approach does not lead to an increased cell voltage [145]. In this case, however, important precursors of some commodity chemicals are formed on both the electrodes. As these products are all in the gas phase, it is easy to separate them from the aqueous electrolyte during a subsequent technological step. This concept is very similar to the so called oxygen depolarized cathode chlor-alkali cells, where chlorine is formed on the anode, while oxygen gas is reduced on the cathode [146]. Plants operating on this concept have been in operation for years; and therefore the infrastructure and technological know-how are readily available. Finally, while H_2 oxidation at the anode is not a value-added approach, it allows for gas feed on both sides, which can be beneficial in certain instances [44,147].

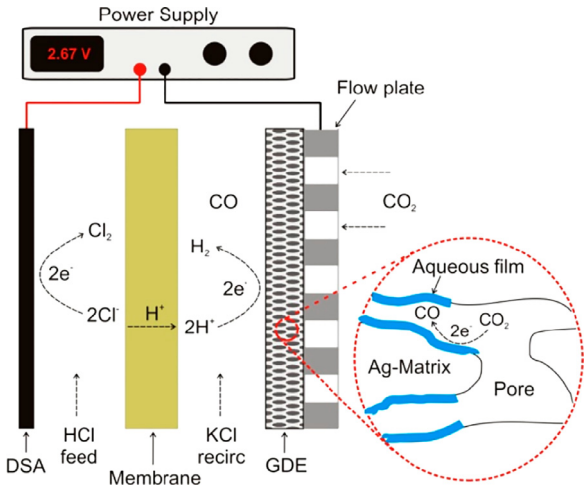

Fig. 21. Schematic illustration of the chlor-syngas electrochemical process. Reproduced with permission from ref. [144].

We are also convinced that concentrated efforts need to be devoted to scale-up and scale-out, to achieve reactor sizes which are at least similar to industrially used water electrolyzers (2 MW). It is worth emphasizing that conclusions drawn for electrochemical cells offering very low current densities are not necessarily valid for those with high currents. Consequently, analyzing electrodes/cells under conditions which are far removed from those which are necessary for practical applications, is a futile exercise. Finally, we hope that the proposed benchmarking protocol will provide insightful guidelines to researchers involved in this endeavor and will lead to more comparable results.

Acknowledgments

This project has received funding from the European Research Council (ERC) under the European Union's Horizon 2020 Research and Innovation Programme (grant agreement No 716539). This work was partly supported by the Momentum Program of the Hungarian Academy of Sciences (LP-2014/3) and the GINOP 2.3.2/2015-13 project. The authors are very thankful to Prof. Paul J. Kenis (University of Illinois at Urban Champaign) for his constructive criticism and insightful comments on an earlier version of this manuscript.

References

[1] Lewis NS, Nocera DG. Powering the planet: Chemical challenges in solar energy utilization. Proc Natl Acad Sci 2006;103:15729–35. doi: 10.1073/pnas.0603395103.
[2] Lewis NS. Research opportunities to advance solar energy utilization. Science 2016;351:353–62. doi: 10.1126/science.aad1920.
[3] Kumar B, Llorente M, Froehlich J, Dang T, Sathrum A, Kubiak CP. Photochemical and photoelectrochemical reduction of CO_2. Annu Rev Phys Chem 2012;63:541–69. doi: 10.1146/annurev-physchem-032511-143759.
[4] Herron JA, Kim J, Upadhye A, Huber GW, Maravelias CT. A general framework for the assessment of solar fuel technologies. Energy Environ Sci 2015;8:126–57. doi: 10.1039/C4EE01958J.
[5] Centi G, Perathoner S. Perspectives and state of the art in producing solar fuels and chemicals from CO_2. In: Centi G, Perathoner S, editors. Green carbon dioxide advances in CO utilization. Wiley Online Library; 2014. p. 1–24. doi: 10.1002/9781118831922.ch1.
[6] Ganesh I. Conversion of carbon dioxide into methanol – a potential liquid fuel: Fundamental challenges and opportunities (a review). Renew Sustain Energy Rev 2014;31:221–57. doi: 10.1016/j.rser.2013.11.045.

[7] Herron JA, Maravelias CT. Assessment of solar-to-fuels strategies : photocatalysis and electrocatalytic reduction. Energy Technol 2016;4:1369–91. doi: 10.1002/ente.201600163.

[8] Nocera DG. The artificial leaf. Acc Chem Res 2012;45:767–76. doi: 10.1021/ar2003013.

[9] Osterloh FE. Photocatalysis versus photosynthesis: a sensitivity analysis of devices for solar energy conversion and chemical transformations. ACS Energy Lett 2017: 445–53. doi: 10.1021/acsenergylett.6b00665.

[10] Usubharatana P, Mcmartin D, Veawab A, Tontiwachwuthikul P. Photocatalytic process for CO_2 emission reduction from industrial flue gas streams. Ind Eng Chem Res 2006;45:2558–68. doi: 10.1021/ie0505763.

[11] "Molly" Jhong H-R, Ma S, Kenis PJ. Electrochemical conversion of CO_2 to useful chemicals: current status, remaining challenges, and future opportunities. Curr Opin Chem Eng 2013;2:191–9. doi: 10.1016/j.coche.2013.03.005.

[12] Costentin C, Robert M, Savéant J-M. Catalysis of the electrochemical reduction of carbon dioxide. Chem Soc Rev 2013;42:2423–36. doi: 10.1039/c2cs35360a.

[13] Boston DJ, Huang KL, de Tacconi NR, Myung N, MacDonnell FM, Rajeshwar K. Electro- and photocatalytic reduction of CO_2: the homogeneous and heterogeneous worlds collide? Photoelectrochemical water splitting : materials, processes and architectures; 2013289–332. doi: 10.1039/9781849737739-00289.

[14] Schmalensee R. The future of solar energy, an interdisciplonary MIT study. Massachussetts Institute of Technology ISBN (978-0-928008-9-8); 2015.

[15] Whipple DT, Kenis PJA. Prospects of CO_2 utilization via direct heterogeneous electrochemical reduction. J Phys Chem Lett 2010;1:3451–8. doi: 10.1021/jz1012627.

[16] Jones JP, Prakash GKS, Olah GA. Electrochemical CO_2 reduction: recent advances and current trends. Isr J Chem 2014;54:1451–66. doi: 10.1002/ijch.201400081.

[17] Kortlever R, Shen J, Schouten KJP, Calle-Vallejo F, Koper MTM. Catalysts and reaction pathways for the electrochemical reduction of carbon dioxide. J Phys Chem Lett 2015;6:4073–82. doi: 10.1021/acs.jpclett.5b01559.

[18] Qiao J, Liu Y, Hong F, Zhang J. A review of catalysts for the electroreduction of carbon dioxide to produce low-carbon fuels. Chem Soc Rev 2014;43:631–75. doi: 10.1039/c3cs60323g.

[19] Kuhl KP, Cave ER, Abram DN, Jaramillo TF. New insights into the electrochemical reduction of carbon dioxide on metallic copper surfaces. Energy Environ Sci 2012;5:7050–9. doi: 10.1039/c2ee21234j.

[20] Janaky C, Hursán D, Endrodi B, Chanmanee W, Roy D, Liu D, et al. Electro- and photoreduction of carbon dioxide : the twain shall meet at copper oxide/copper nanocube interfaces. ACS Energy Lett 2016;1:332–8. doi: 10.1021/acsenergylett.6b00078.

[21] Verma S, Kim B, "Molly JhongH-R, Ma S, Kenis PJA. A gross-margin model for defining technoeconomic benchmarks in the electroreduction of CO_2. ChemSusChem 2016;9:1972–9. doi: 10.1002/cssc.201600394.

[22] Martín AJ, Larrazábal GO, Pérez-Ramírez J. Towards sustainable fuels and chemicals through the electrochemical reduction of CO_2 : lessons from water electrolysis. Green Chem 2015;17:5114–30. doi: 10.1039/C5GC01893E.

[23] Wong CS, Tishchenko PY, Johnson WK. Solubility of carbon dioxide in aqueous HCl and $NaHCO_3$ solutions from 278 to 298 K. J Chem Eng Data 2005;50:817–21. doi: 10.1021/je049716q.

[24] Dewulf DW, Bard AJ. The electrochemical reduction of CO_2 to CH_4 and C_2H_4 at Cu/Nafion electrodes (solid polymer electrolyte structures). Catal Letters 1988;1:73–80. doi: 10.1007/BF00765357.

[25] Bevilacqua M, Filippi J, Miller HA, Vizza F. Recent technological progress in CO_2 electroreduction to fuels and energy carriers in aqueous environments. Energy Technol 2015;3:197–210. doi: 10.1002/ente.201402166.

[26] Albo J, Alvarez-Guerra M, Castaño P, Irabien A. Towards the electrochemical conversion of carbon dioxide into methanol. Green Chem 2015;17:2304–24. doi: 10.1039/C4GC02453B.

[27] Merino-Garcia I, Alvarez-Guerra E, Albo J, Irabien A. Electrochemical membrane reactors for the utilisation of carbon dioxide. Chem Eng J 2016;305:104–20. doi: 10.1016/j.cej.2016.05.032.

[28] Kondratenko E V, Mul G, Baltrusaitis J, Larrazabal GO, Perez-Ramirez J, Larrazábal GO, et al. Status and perspectives of CO_2 conversion into fuels and chemicals by catalytic, photocatalytic and electrocatalytic processes. Energy Environ Sci 2013;6:3112–35. doi: 10.1039/c3ee41272e.

[29] Lobaccaro P, Singh MR, Clark L, Kwon Y, Bell AT, Ager JW. Effects of temperature and gas – liquid mass transfer on the operation of small electrochemical cells for the quantitative evaluation of CO_2 reduction electrocatalysts. Phys Chem Chem Phys 2016;18:26777–85. doi: 10.1039/C6CP05287H.

[30] Singh MR, Clark EL, Bell AT. Effects of electrolyte, catalyst, and membrane composition and operating conditions on the performance of solar-driven electrochemical reduction of carbon dioxide. Phys Chem Chem Phys 2015;17:18924–36. doi: 10.1039/C5CP03283K.

[31] Kas R, Hummadi KK, Kortlever R, de Wit P, Milbrat A, Luiten-Olieman MWJ, et al. Three-dimensional porous hollow fibre copper electrodes for efficient and high-rate electrochemical carbon dioxide reduction. Nat Commun 2016;7:10748–54. doi: 10.1038/ncomms10748.

[32] Darvas F, Hessel V, György D. Flow chemistry - Fundamentals. 1st ed. De Gruyter ISBN 978-3-11-028916-9; 2014.

[33] Ma S, Sadakiyo M, Luo R, Heima M, Yamauchi M, Kenis PJA. One-step electrosynthesis of ethylene and ethanol from CO_2 in an alkaline electrolyzer. J Power Sources 2016;301:219–28. doi: 10.1016/j.jpowsour.2015.09.124.

[34] Hereijgers J, Ottevaere H, Breugelmans T, De Malsche W. Membrane deflection in a flat membrane microcontactor : experimental study of spacer features. J Membr Sci 2016;504:153–61. doi: 10.1016/j.memsci.2016.01.015.

[35] Whipple DT, Finke EC, Kenis PJA. Microfluidic reactor for the electrochemical reduction of carbon dioxide: the effect of pH. Electrochem Solid-State Lett 2010;13:B109–11. doi: 10.1149/1.3456590.

[36] Tornow CE, Thorson MR, Ma S, Gewirth AA, Kenis PJA. Nitrogen-based catalysts for the electrochemical reduction of CO_2 to CO. J Am Chem Soc 2012;134:19520–3. doi: 10.1021/ja308217w.

[37] Lu X, Leung DYC, Wang H, Xuan J. A high performance dual electrolyte microfluidic reactor for the utilization of CO_2. Appl Energy 2017;194:549–59. doi: 10.1016/j.apenergy.2016.05.091.

[38] Ma S, Luo R, Gold JI, Yu AZ, Kim B, Kenis PJA. Carbon nanotube containing Ag catalyst layers for efficient and selective reduction of carbon dioxide. J Mater Chem A 2016;4:8573–8. doi: 10.1039/C6TA00427J.

[39] Verma S, Lu X, Ma S, Masel RI, Kenis PJA. The effect of electrolyte composition on the electroreduction of CO_2 to CO on Ag based gas diffusion electrodes. Phys Chem Chem Phys 2015;18:7075–84. doi: 10.1039/C5CP05665A.

[40] Alvarez-Guerra M, Del Castillo A, Irabien A. Continuous electrochemical reduction of carbon dioxide into formate using a tin cathode: Comparison with lead cathode. Chem Eng Res Des 2014;92:692–701. doi: 10.1016/j.cherd.2013.11.002.

[41] Merino García I, Albo J, Irabien A. Productivity and selectivity of gas phase CO_2 electroreduction to methane at Cu nanoparticle-based electrodes. Energy Technol 2017. in press doi: 10.1002/ente.201600616.

[42] Cook RL, MacDuff RC, Sammells AF. High rate gas phase CO_2 reduction to ethylene and methane using gas diffusion electrodes. J Electrochem Soc 1990;137:607–8. doi: 10.1149/1.2086515.

[43] Gutierrez-Guerra N, Moreno-Lopez L, Serrano-Ruiz JC, Valverde JL, de Lucas-Consuegra A. Gas phase electrocatalytic conversion of CO_2 to syn-fuels on Cu based catalysts-electrodes. Appl Catal B Environ 2016;188:272–82. doi: 10.1016/j.apcatb.2016.02.010.

[44] Pérez-Rodríguez S, Barreras F, Pastor E, Lázaro MJ. Electrochemical reactors for CO_2 reduction: From acid media to gas phase. Int J Hydrogen Energy 2016;41:19756–65. doi: 10.1016/j.ijhydene.2016.06.130.

[45] Li G, Pickup PG. Measurement of single electrode potentials and impedances in hydrogen and direct methanol PEM fuel cells. Electrochim Acta 2004;49:4119–26. doi: 10.1016/j.electacta.2004.04.005.

[46] Herrera OE, Merida W, Wilkinson DP. New reference electrode approach for fuel cell performance evaluation. ECS Trans 2008;16:1915–26. doi: 10.1149/1.2982032.

[47] Kulikovsky AA, Berg P. Positioning of a reference electrode in a PEM fuel cell. J Electrochem Soc 2015;162:F843–8. doi: 10.1149/2.0231508jes.

[48] Liu Z, Wainright JS, Huang W, Savinell RF. Positioning the reference electrode in proton exchange membrane fuel cells: calculations of primary and secondary current distribution. Electrochim Acta 2004;49:923–35. doi: 10.1016/j.electacta.2003.10.004.

[49] Garg G, Basu S. Studies on degradation of copper nano particles in cathode for CO_2 electrolysis to organic compounds. Electrochim Acta 2015;177:359–65. doi: 10.1016/j.electacta.2015.03.161.

[50] Albo J, Sáez A, Solla-Gullón J, Montiel V, Irabien A. Production of methanol from CO_2 electroreduction at Cu_2O and Cu_2O/ZnO-based electrodes in aqueous solution. Appl Catal B Environ 2015;176:709–17. doi: 10.1016/j.apcatb.2015.04.055.

[51] Wu J, Risalvato FG, Sharma PP, Pellechia PJ, Ke F-S, Zhou X-D. Electrochemical reduction of carbon dioxide: II. Design, assembly, and performance of low temperature full electrochemical cells. J Electrochem Soc 2013;160:F953–7. doi: 10.1149/2.030309jes.

[52] Aeshala LM, Rahman SU, Verma A. Effect of solid polymer electrolyte on electrochemical reduction of CO_2. Sep Purif Technol 2012;94:131–7. doi: 10.1016/j.seppur.2011.12.030.

[53] Liua Z, Masel RI, Chen Q, Kutz R, Yang H, Lewinski K, et al. Electrochemical generation of syngas from water and carbon dioxide at industrially important rates. J CO_2 Util 2016;15:50–6. doi: 10.1016/j.jcou.2016.04.011.

[54] Li H, Oloman C. Development of a continuous reactor for the electro-reduction of carbon dioxide to formate – Part 2: Scale-up. J Appl Electrochem 2007;37:1107–17. doi: 10.1007/s10800-007-9371-8.

[55] Oloman C, Li H. Electrochemical processing of carbon dioxide. ChemSusChem 2008;1:385–91. doi: 10.1002/cssc.200800015.

[56] Albo J, Vallejo D, Beobide G, Castillo O, Castaño P, Irabien A. Copper-based metal-organic porous materials for CO_2 electrocatalytic reduction to alcohols. ChemSusChem 2017;10:1100–9. doi: 10.1002/cssc.201600693.

[57] Luc W, Rosen J, Jiao F. An Ir-based anode for a practical CO_2 electrolyzer. Catal Today 2016: 1–6. doi: 10.1016/j.cattod.2016.06.011.

[58] Jhong HRQ, Brushett FR, Kenis PJA. The effects of catalyst layer deposition methodology on electrode performance. Adv Energy Mater 2013;3:589–99. doi: 10.1002/aenm.201200759.

[59] Dufek EJ, Lister TE, Mcllwain ME. Bench-scale electrochemical system for generation of CO and syn-gas. J Appl Electrochem 2011;41:623–31. doi: 10.1007/s10800-011-0271-6.

[60] Dufek EJ, Lister TE, Stone SG, Mcilwain ME. Operation of a pressurized system for continuous reduction of CO_2. J Electrochem Soc 2012;159:514–7. doi: 10.1149/2.011209jes.

[61] Ma S, Lan Y, Perez GMJ, Moniri S, Kenis PJA. Silver supported on titania as an active catalyst for electrochemical carbon dioxide reduction. ChemSusChem 2014;7:866–74. doi: 10.1002/cssc.201300934.

[62] Shi J, Li Q-Y, Shi F, Song N, Jia Y-J, Hu Y-Q, et al. Design of a two-compartment electrolysis cell for the reduction of CO_2 to CO in tetrabutylammonium perchlorate/propylene carbonate for renewable electrical energy storage. J Electrochem Soc 2016;163:G82–7. doi: 10.1149/2.1381607jes.

[63] Stevens GB, Reda T, Raguse B. Energy storage by the electrochemical reduction of CO_2 to CO at a porous Au film. J Electroanal Chem 2002;526:125–33. doi: 10.1016/S0022-0728(02)00688-5.

[64] Komatsu S, Tanaka M, Okumura A, Kungi A. Preparation of Cu-solid polymer electrolyte composite electrodes and application to gas-phase electrochemical reduction of CO_2. Electrochim Acta 1995;40:745–53. doi: 10.1016/0013-4686(94)00325-U.

[65] Lan Y, Gai C, Kenis PJA, Lu J. Electrochemical reduction of carbon dioxide on Cu/CuO core/shell catalysts. ChemElectroChem 2014;1:1577–82. doi: 10.1002/celc.201402182.

[66] Aeshala LM, Uppaluri RG, Verma A. Effect of cationic and anionic solid polymer electrolyte on direct electrochemical reduction of gaseous CO_2 to fuel. J CO_2 Util 2013;3–4:49–55. doi: 10.1016/j.jcou.2013.09.004.

[67] Albo J, Irabien A. Cu_2O-loaded gas diffusion electrodes for the continuous electrochemical reduction of CO_2 to methanol. J Catal 2016;343:232–9. doi: 10.1016/j.jcat.2015.11.014.

[68] Homayoni H, Chanmanee W, de Tacconi NR, Dennis BH, Rajeshwar K, Homayon H, et al. Continuous flow photoelectrochemical reactor for solar conversion of carbon dioxide to alcohols. J Electrochem Soc 2015;162:E115–22. doi: 10.1149/2.0331508jes.

[69] Wang Q, Dong H, Yu H, Yu H, Liu M. Enhanced electrochemical reduction of carbon dioxide to formic acid using a two-layer gas diffusion electrode in a microbial electrolysis cell. RSC Adv 2015;5:10346–51. doi: 10.1039/C4RA14535F.

[70] Li H, Oloman C. Development of a continuous reactor for the electro-reduction of carbon dioxide to formate - Part 1: Process variables. J Appl Electrochem 2006;36:1105–15. doi: 10.1007/s10800-007-9371-8.

[71] Li H, Oloman C. The electro-reduction of carbon dioxide in a continuous reactor. J Appl Electrochem 2005;35:955–65. doi: 10.1007/s10800-005-7173-4.

[72] Kopljar D, Wagner N, Klemm E. Transferring electrochemical CO_2 reduction from semi-batch into continuous operation mode using gas diffusion electrodes. Chem Eng Technol 2016;39:2042–50. doi: 10.1002/ceat.201600198.

[73] MacHunda RL, Lee J, Lee J. Microstructural surface changes of electrodeposited Pb on gas diffusion electrode during electroreduction of gas-phase CO_2. Surf Interface Anal 2010;42:564–7. doi: 10.1002/sia.3245.

[74] Lu X, Leung DYC, Wang H, Maroto-Valer MM, Xuan J. A pH-differential dual-electrolyte microfluidic electrochemical cells for CO_2 utilization. Renew Energy 2016;95:277–85. doi: 10.1016/j.renene.2016.04.021.

[75] Genovese C, Ampelli C, Perathoner S, Centi G. Electrocatalytic conversion of CO_2 on carbon nanotube-based electrodes for producing solar fuels. J Catal 2013;308:237–49. doi: 10.1016/j.jcat.2013.08.026.

[76] White JL, Herb JT, Kaczur JJ, Majsztrik PW, Bocarsly AB. Photons to formate: Efficient electrochemical solar energy conversion via reduction of carbon dioxide. J CO_2 Util 2014;7:1–5. doi: 10.1016/j.jcou.2014.05.002.

[77] Centi G, Perathoner S, Wine G, Gangeri M. Electrocatalytic conversion of CO_2 to long carbon-chain hydrocarbons. Green Chem 2007;9:671–8. doi: 10.1039/b615275a.

[78] Wu J, Sharma PP, Harris BH, Zhou X. Electrochemical reduction of carbon dioxide : IV dependence of the Faradaic efficiency and current density on the microstructure and thickness of tin electrode. J Power Sources 2014;258:189–94. doi: 10.1016/j.jpowsour.2014.02.014.

[79] Lu Q, Rosen J, Jiao F. Nanostructured metallic electrocatalysts for carbon dioxide reduction. ChemCatChem 2015;7:38–47. doi: 10.1002/cctc.201402669.

[80] Manthiram K, Beberwyck BJ, Alivisatos AP. Enhanced electrochemical methanation of carbon dioxide with a dispersible nanoscale copper catalyst. J Am Chem Soc 2014;136:13319–25. doi: 10.1021/ja5065284.

[81] Bevilacqua M, Filippi J, Folliero M, Lavacchi A, Miller HA, Marchionni A, et al. Enhancement of the efficiency and selectivity for carbon dioxide electroreduction to fuels on tailored copper catalyst architectures. Energy Technol 2016;4:1020–8. doi: 10.1002/ente.201600044.

[82] Del Castillo A, Alvarez-Guerra M, Solla-Gullón J, Sáez A, Montiel V, Irabien A. Electrocatalytic reduction of CO_2 to formate using particulate Sn electrodes: Effect of metal loading and particle size. Appl Energy 2015;157:165–73. doi: 10.1016/j.apenergy.2015.08.012.

[83] Bitar Z, Fecant A, Trela-Baudot E, Chardon-Noblat S, Pasquier D. Electrocatalytic reduction of carbon dioxide on indium coated gas diffusion electrodes-Comparison with indium foil. Appl Catal B Environ 2016;189:172–80. doi: 10.1016/j.apcatb.2016.02.041.

[84] Kim B, Hillman F, Ariyoshi M, Fujikawa S, Kenis PJA. Effects of composition of the micro porous layer and the substrate on performance in the electrochemical reduction of CO_2 to CO. J Power Sources 2016;312:192–8. doi: 10.1016/j.jpowsour.2016.02.043.

[85] Irtem E, Andreu T, Parra A, Hernandez-Alonso MD, García-Rodríguez S, Riesco García JM, et al. Low-energy formate production from CO_2 electroreduction using electrodeposited tin on GDE. J Mater Chem A 2016;4:13582–8. doi: 10.1039/C6TA04432H.

[86] Antolini E, Giorgi L, Pozio A, Passalacqua E. Influence of Nafion loading in the catalyst layer of gas-diffusion electrodes for PEFC. J Power Sources 1999;77:136–42. doi: 10.1016/S0378-7753(98)00186-4.

[87] Jeon S, Lee J, Rios GM, Kim H-J, Lee S-Y, Cho E, et al. Effect of ionomer content and relative humidity on polymer electrolyte membrane fuel cell (PEMFC) performance of membrane-electrode assemblies (MEAs) prepared by decal transfer method. Int J Hydrogen Energy 2010;35:9678–86. doi: 10.1016/j.ijhydene.2010.06.044.

[88] Liu Y, Murphy MW, Baker DR, Gu W, Ji C, Jorne J, et al. Proton conduction and oxygen reduction kinetics in PEM fuel cell cathodes: Effects of ionomer-to-carbon ratio and relative humidity. J Electrochem Soc 2009;156:B970–80. doi: 10.1149/1.3143965.

[89] Wilson MS, Gottesfeld S. Thin-film catalyst layers for polymer electrolyte fuel cell electrodes. J Appl Electrochem 1992;22:1–7. doi: 10.1007/BF01093004.

[90] Narayanan SR, Haines B, Soler J, Valdez TI. Electrochemical conversion of carbon dioxide to formate in alkaline polymer electrolyte membrane cells. J Electrochem Soc 2011;158:A167–73. doi: 10.1149/1.3526312.

[91] Oh Y, Hu X. Organic molecules as mediators and catalysts for photocatalytic and electrocatalytic CO_2 reduction. Chem Soc Rev 2013;42:2253–61. doi: 10.1039/c2cs35276a.

[92] Xia Z, Qiu W, Bao H, Yang B, Lei L, Xu Z, et al. Electrochemical reduction of gaseous CO_2 with a catechol and polyethyleneimine co-deposited polypropylene membrane. Electrochem Commun 2016;71:1–4. doi: 10.1016/j.elecom.2016.07.009.

[93] Robert A, Kutz B, Chen Q, Yang H, Dawar S, Liu Z, et al. Sustainion™ imidazolium functionalized polymers for CO_2 electrolysis. Energy Technol 2017. doi: 10.1002/ente.201600636 in press.

[94] Hori Y, Ito H, Okano K, Nagasu K, Sato S. Silver-coated ion exchange membrane electrode applied to electrochemical reduction of carbon dioxide. Electrochim Acta 2003;48:2651–7. doi: 10.1016/S0013-4686(03)00311-6.

[95] Sun K, Liu R, Chen Y, Verlage E, Lewis NS, Xiang C. A stabilized, intrinsically safe, 10% efficient, solar-driven water-splitting cell incorporating earth-abundant electrocatalysts with steady-state pH gradients and product separation enabled by a bipolar membrane. Adv Energy Mater 2016;6:1600379. doi: 10.1002/aenm.201600379.

[96] Luo J, Vermaas DA, Bi D, Hagfeldt A, Smith WA, Grätzel M. Bipolar membrane-assisted solar water splitting in optimal pH. Adv Energy Mater 2016;6:1600100. doi: 10.1002/aenm.201600100.

[97] Li X, Sabir I. Review of bipolar plates in PEM fuel cells: Flow-field designs. Int J Hydrogen Energy 2005;30:359–71. doi: 10.1016/j.ijhydene.2004.09.019.

[98] Ito H, Maeda T, Nakano A, Hasegawa Y, Yokoi N, Hwang CM, et al. Effect of flow regime of circulating water on a proton exchange membrane electrolyzer. Int J Hydrogen Energy 2010;35:9550–60. doi: 10.1016/j.ijhydene.2010.06.103.

[99] Kim H-Y, Choi I, Ahn SH, Hwang SJ, Yoo SJ, Han J, et al. Analysis on the effect of operating conditions on electrochemical conversion of carbon dioxide to formic acid. Int J Hydrogen Energy 2014;39:16506–12. doi: 10.1016/j.ijhydene.2014.03.145.

[100] Thorson MR, Siil KI, Kenis PJA. Effect of cations on the electrochemical conversion of CO_2 to CO. J Electrochem Soc 2013;160:F69–74. doi: 10.1149/2.052301jes.

[101] Ma S, Luo R, Moniri S, Lan Y, Kenis PJA. Efficient electrochemical flow system with improved anode for the conversion of CO_2 to CO. J Electrochem Soc 2014;161:F1124–31. doi: 10.1149/2.1201410jes.

[102] Kopljar D, Inan A, Vindayer P, Wagner N, Klemm E. Electrochemical reduction of CO_2 to formate at high current density using gas diffusion electrodes. J Appl Electrochem 2014;44:1107–16. doi: 10.1007/s10800-014-0731-x.

[103] Dufek EJ, Lister TE, Stone SG. Sampling dynamics for pressurized electrochemical cells. J Appl Electrochem 2014;44:849–55. doi: 10.1007/s10800-014-0693-z.

[104] Schwartz M, Cook RL, Kehoe VM, MacDuff RC, Patel J, Sammells AF. Carbon dioxide reduction to alcohols using perovskite-type electrocatalysts. J Electrochem Soc 1993;140:614–8. doi: 10.1149/1.2056131.

[105] Bumroongsakulsawat P, Kelsall GH. Tinned graphite felt cathodes for scale-up of electrochemical reduction of aqueous CO_2. Electrochim Acta 2015;159:242–51. doi: 10.1016/j.electacta.2015.01.209.

[106] Jhong H-RM, Tornow CE, Smid B, Gewirth AA, Lyth SM, Kenis PJA. A nitrogen-doped carbon catalyst for electrochemical CO_2 conversion to CO with high selectivity and current density. ChemSusChem 2017;10:1094–9. doi: 10.1002/cssc.201600843.

[107] Delacourt C, Ridgway PL, Kerr JB, Newman J. Design of an electrochemical cell making syngas ($CO+H_2$) from CO_2 and H_2O reduction at room temperature. J Electrochem Soc 2008;155:B42–9. doi: 10.1149/1.2801871.

[108] Alvarez-Guerra M, Albo J, Alvarez-Guerra E, Irabien A. Ionic liquids in the electrochemical valorisation of CO_2. Energy Environ Sci 2015;8:2574–99. doi: 10.1039/C5EE01486G.

[109] Rosen BA, Salehi-khojin A, Thorson MR, Zhu W, Whipple DT, Kenis PJA, et al. Ionic liquid–mediated selective conversion of CO_2 to CO at low overpotentials. Science 2011;334:643–4 doi: science.1209786/DC1.

[110] Sen S, Liu D, Palmore TR. Electrochemical reduction of CO_2 at copper nanofoams. ACS Catal 2014;4:3091–5. doi: 10.1021/cs500522g.

[111] Kriescher SMA, Kugler K, Hosseiny SS, Gendel Y, Wessling M. A membrane electrode assembly for the electrochemical synthesis of hydrocarbons from $CO_{2(g)}$ and $H_2O_{(g)}$. Electrochem Commun 2015;50:64–8. doi: 10.1016/j.elecom.2014.11.014.

[112] Wang Q, Dong H, Yu H. Development of rolling tin gas diffusion electrode for carbon dioxide electrochemical reduction to produce formate in aqueous electrolyte. J Power Sources 2014;271:278–84. doi: 10.1016/j.jpowsour.2014.08.017.

[113] Agarwal AS, Zhai Y, Hill D, Sridhar N. The electrochemical reduction of carbon dioxide to formate/formic acid: engineering and economic feasibility. ChemSusChem 2011;4:1301–10. doi: 10.1002/cssc.201100220.

[114] McCrory CCL, Jung S, Peters JC, Jaramillo TF. Benchmarking heterogeneous electrocatalysts for the oxygen evolution reaction. J Am Chem Soc 2013;135:16977–87. doi: 10.1021/ja407115p.

[115] Gasteiger HA, Kocha SS, Sompalli B, Wagner FT. Activity benchmarks and requirements for Pt, Pt-alloy, and non-Pt oxygen reduction catalysts for PEMFCs. Appl Catal B Environ 2005;56:9–35. doi: 10.1016/j.apcatb.2004.06.021.
[116] Makharia R, Kocha S, Yu P, Sweikart MA, Gu W, Wagner F, et al. Durable PEM fuel cell electrode materials: Requirements and benchmarking methodologies. ECS Trans 2006;1:3–18. doi: 10.1149/1.2214540.
[117] Chen Z, Jaramillo TF, Deutsch TG, Kleiman-Shwarsctein A, Forman AJ, Gaillard N, et al. Accelerating materials development for photoelectrochemical hydrogen production: Standards for methods, definitions, and reporting protocols. J Mater Res 2010;25:3–16. doi: 10.1557/JMR.2010.0020.
[118] McCrory CCL, Jung S, Ferrer IM, Chatman SM, Peters JC, Jaramillo TF. Benchmarking hydrogen evolving reaction and oxygen evolving reaction electrocatalysts for solar water splitting devices. J Am Chem Soc 2015;137:4347–57. doi: 10.1021/ja510442p.
[119] Doña Rodríguez JM, Herrera Melián JA, Pérez Peña J. Determination of the real surface area of Pt electrodes by hydrogen adsorption using cyclic voltammetry. J Chem Educ 2000;77:1195–7. doi: 10.1021/ed077p1195.
[120] Hsieh Y-C, Senanayake SD, Zhang Y, Xu W, Polyansky DE. Effect of chloride anions on the synthesis and enhanced catalytic activity of silver nanocoral electrodes for CO_2 electroreduction. ACS Catal 2015;5:5349–56. doi: 10.1021/acscatal.5b01235.
[121] Yuan X, Wang H, Colinsun J, Zhang J. AC impedance technique in PEM fuel cell diagnosis—a review. Int J Hydrogen Energy 2007;32:4365–80. doi: 10.1016/j.ijhydene.2007.05.036.
[122] van der Vliet D, Strmcnik DS, Wang C, Stamenkovic VR, Markovic NM, Koper MTM. On the importance of correcting for the uncompensated Ohmic resistance in model experiments of the Oxygen Reduction Reaction. J Electroanal Chem 2010;647:29–34. doi: 10.1016/j.jelechem.2010.05.016.
[123] Pougin A, Dilla M, Strunk J. Identification and exclusion of intermediates of photocatalytic CO_2 reduction on TiO_2 under conditions of highest purity. Phys Chem Chem Phys 2016;18:3–4. doi: 10.1039/C5CP07148H.
[124] Huang L, Sorte EG, Sun S, Tong YYJ. A straightforward implementation of in situ solution electrochemical ^{13}C NMR spectroscopy for studying reactions on commercial electrocatalysts: ethanol oxidation. Chem Commun 2015;51:8086–8. doi: 10.1039/C5CC00862J.
[125] Clark EL, Singh MR, Kwon Y, Bell AT. Differential electrochemical mass spectrometer cell design for online quantification of products produced during electrochemical reduction of CO_2. Anal Chem 2015;87:8013–20. doi: 10.1021/acs.analchem.5b02080.
[126] Del Castillo A, Alvarez-Guerra M, Irabien A. Continuous electroreduction of CO_2 to formate using Sn gas diffusion electrodes. AIChE J 2014;60:3557–64. doi: 10.1002/aic.14544.
[127] Shao Y, Yin G, Gao Y. Understanding and approaches for the durability issues of Pt-based catalysts for PEM fuel cell. J Power Sources 2007;171:558–66. doi: 10.1016/j.jpowsour.2007.07.004.
[128] Wu J, Sun SG, Zhou XD. Origin of the performance degradation and implementation of stable tin electrodes for the conversion of CO_2 to fuels. Nano Energy 2016;27:225–9. doi: 10.1016/j.nanoen.2016.06.028.
[129] Zeng K, Zhang D. Recent progress in alkaline water electrolysis for hydrogen production and applications. Prog Energy Combust Sci 2010;36:307–26. doi: 10.1016/j.pecs.2009.11.002.
[130] Ferreira RB, Falcão DS, Oliveira VB, Pinto AMFR. Experimental study on the membrane electrode assembly of a proton exchange membrane fuel cell: effects of microporous layer, membrane thickness and gas diffusion layer hydrophobic treatment. Electrochim Acta 2017;224:337–45. doi: 10.1016/j.electacta.2016.12.074.
[131] White JL, Baruch MF, Pander JE, Hu Y, Fortmeyer IC, Park JE, et al. Light-driven heterogeneous reduction of carbon dioxide: photocatalysts and photoelectrodes. Chem Rev 2015;115:12888–935. doi: 10.1021/acs.chemrev.5b00370.
[132] Ampelli C, Centi G, Passalacqua R, Perathoner S. Electrolyte-less design of PEC cells for solar fuels: prospects and open issues in the development of cells and related catalytic electrodes. Catal Today 2016;259:246–58. doi: 10.1016/j.cattod.2015.07.020.
[133] Rajeshwar K. Electron transfer at semiconductor–electrolyte interfaces. In: Balzani V, editor. Electron transfer in chemistry. Weinheim: Wiley- VCH; 2001. doi: 10.1002/9783527618248.ch53.
[134] Gimenez S, Bisquert J. Photoelectrochemical solar fuel production, from basic principles to advanced devices. Springer; 2016. doi: 10.1007/978-3-319-29641-8.
[135] Thompson JF, Chen B, Kubo M, Londono N, Minuzzo J. Artificial photosynthesis device development for CO_2 photoelectrochemical conversion. MRS Adv 2016;1:447–52. doi: 10.1557/adv.2016.111.
[136] Ampelli C, Centi G, Passalacqua R, Perathoner S. Synthesis of solar fuels by a novel photoelectrocatalytic approach. Energy Environ Sci 2010;3:292–301. doi: 10.1039/c003390c.
[137] Parkinson B. On the efficiency and stability of photoelectrochemical devices. Acc Chem Res 1984;17:431–7. doi: 10.1021/ar00108a004.
[138] Walter MG, Warren EL, McKone JR, Boettcher SW, Mi Q, Santori EA, et al. Solar water splitting cells. Chem Rev 2010;110:6446–73. doi: 10.1021/cr1002326.
[139] Chen Z, Dinh HN, Miller E. Photoelectrochemical water splitting. New York: Springer Briefs in Energy; 2013. doi: 10.1007/978-1-4614-8298-7.
[140] Herranz J, Durst J, Fabbri E, Patru A, Cheng X, Permyakova AA, et al. Interfacial effects on the catalysis of the hydrogen evolution, oxygen evolution and CO_2-reduction reactions for (co-)electrolyzer development. Nano Energy 2016;29:4–28. doi: 10.1016/j.nanoen.2016.01.027.
[141] Hudkins JR, Wheeler DG, Pen B, Berlinguette CP. Rapid prototyping of electrolyzer flow field plates. Energy Environ Sci 2016;9:3417–23. doi: 10.1039/C6EE01997H.
[142] Sabatino S, Galia A, Saracco G, Scialdone O. Development of an electrochemical process for the simultaneous treatment of wastewater and the conversion of carbon dioxide to higher value products. ChemElectroChem 2017;4:150–9. doi: 10.1002/celc.201600475.
[143] Martínez-Huitle CA, Ferro S. Electrochemical oxidation of organic pollutants for the wastewater treatment: direct and indirect processes. Chem Soc Rev 2006;35:1324–40. doi: 10.1039/B517632H.
[144] Lister TE, Dufek EJ. Chlor-syngas: Coupling of electrochemical technologies for production of commodity chemicals. Energy Fuels 2013;27:4244–9. doi: 10.1021/ef302033j.
[145] Karlsson RKB, Cornell A. Selectivity between oxygen and chlorine evolution in the chlor-alkali and chlorate processes. Chem Rev 2016;116:2982–3028. doi: 10.1021/acs.chemrev.5b00389.
[146] Moussallem I, Jörissen J, Kunz U, Pinnow S, Turek T. Chlor-alkali electrolysis with oxygen depolarized cathodes: history, present status and future prospects. J Appl Electrochem 2008;38:1177–94. doi: 10.1007/s10800-008-9556-9.
[147] Wu J, Risalvato FG, Ma S, Zhou X-D. Electrochemical reduction of carbon dioxide III. The role of oxide layer thickness on the performance of Sn electrode in a full electrochemical cell. J Mater Chem A 2014;2:1647–51. doi: 10.1039/c3ta13544f.